HHS Public Access

Author manuscript

Hear Res. Author manuscript; available in PMC 2022 September 15.

Published in final edited form as:

Hear Res. 2021 September 15; 409: 108327. doi:10.1016/j.heares.2021.108327.

CACHD1-deficient mice exhibit hearing and balance deficits associated with a disruption of calcium homeostasis in the inner ear

Cong Tian[a,c], **Kenneth R. Johnson**[a], **Jaclynn M. Lett**[b], **Robert Voss**[b], **Alec N. Salt**[b], **Jared J. Hartsock**[b], **Peter S. Steyger**[c], **Kevin K. Ohlemiller**[b,*]

[a]The Jackson Laboratory, Bar Harbor, ME, 04609, USA

[b]Department of Otolaryngology, Central Institute for the Deaf, Fay and Carl Simons Center for Hearing and Deafness, Washington University School of Medicine, 660 S. Euclid, Saint Louis MO, 63110, USA

[c]Department of Biomedical Sciences, School of Medicine, Creighton University, 2500 California Plaza, Omaha, NE, 68178, USA

Abstract

CACHD1 recently was shown to be an $\alpha 2\delta$-like subunit that can modulate the activity of some types of voltage-gated calcium channels, including the low-voltage activated, T-type Ca_V3 channels. CACHD1 is widely expressed in the central nervous system but its biological functions and relationship to disease states are unknown. Here, we report that mice with deleterious *Cachd1* mutations are hearing impaired and have balance defects, demonstrating that CACHD1 is functionally important in the peripheral auditory and vestibular organs of the inner ear. The vestibular dysfunction of *Cachd1* mutant mice, exhibited by leaning and head tilting behaviors, is related to a deficiency of calcium carbonate crystals (otoconia) in the saccule and utricle. The auditory dysfunction, shown by ABR threshold elevations and reduced DPOAEs, is associated with reduced endocochlear potentials and increased endolymph calcium concentrations. Paint-fills of mutant inner ears from prenatal and newborn mice revealed dilation of the membranous labyrinth caused by an enlarged volume of endolymph. These pathologies all can be re lated to a disturbance of calcium homeostasis in the endolymph of the inner ear, presumably caused by the loss of CACHD1 regulatory effects on voltage-gated calcium channel activity. *Cachd1* expression in the cochlea appears stronger in late embryonic stages than in adults, suggesting an early role in establishing endolymph calcium concentrations. Our findings provide new insights into CACHD1 function and suggest the involvement of voltage-gated calcium channels in endolymph homeostasis, essential for normal auditory and vestibular function.

*Corresponding author.

Declaration of competing interest

The authors declare no competing financial interests.

Supplementary materials

Supplementary material associated with this article can be found, in the online version, at doi:10.1016/j.heares.2021.108327.

Keywords

Mouse; Cochlea; Endolymph; Endocochlear potential; Macula; Otolith

Introduction

A new recessive mouse mutation that arose spontaneously at The Jackson Laboratory (JAX) was named tilt-o-whirl (*tow*) because of the circling behavior of homozygous mutant mice. Mutant mice also showed head tilting behavior and were unable to swim (K.R. Johnson, unpublished). The *tow* mutation was shown to be recessive by results from crosses of mutant mice with wild-type C57BL/6J (B6) strain mice, which failed to produce any mutant progeny. In addition to vestibular deficits, mutant mice (presumed *tow/tow* genotype) also exhibit variable hearing impairment as assessed by auditory brainstem response (ABR) threshsold analysis. The cache domain containing 1 protein (CACHD1) recently was shown to be an auxiliary subunit of voltage-gated calcium channels (Cottrell et al., 2018; Dahimene et al., 2018; Stephens and Cottrell, 2019). The CACHD1 protein contains two cache domains and one VWFA domain and is similar to the alpha-2/delta ($\alpha_2\delta$) subunit of voltage-gated Ca^{2+} (Ca_v) channels (Anantharaman and Aravind, 2000). The $\alpha_2\delta$ auxiliary subunit can have a marked effect on the trafficking and functional properties of Ca_v channels (Davies et al., 2007; Dolphin, 2016). CACHD1 was shown to be widely expressed in the central nervous system and to specifically modulate low-voltage activated, T-type Ca_v3 channels (Cottrell et al., 2018). In contrast to Ca_v1 and Ca_v2 channels, Ca_v3 channels are not known to associate with $\alpha_2\delta$ subunits (Dolphin, 2016), suggesting that CACHD1 may serve this role. Another recent study found that CACHD1 competes with $\alpha_2\delta_1$ subunits to increase N-type $Ca_v2.2$ channel currents and cell surface trafficking (Dahimene et al., 2018).

Although CACHD1 expression has been reported in cells of the central nervous system, it also may be expressed in cells of peripheral organs that contain calcium channels, such as the inner ear. High-voltage activated, L-type Ca_v1 channels are expressed in the inner ear and include $Ca_v1.3$ channels, which are responsible for the presynaptic activity of cochlear inner hair cells (Platzer et al., 2000; Brandt et al., 2003), and $Ca_v1.2$ and $Ca_v1.3$ channels, which are expressed in spiral ganglion neurons (Lv et al., 2014). The $\alpha_2\delta_2$ subunit (CACNA2D2) co-assembles with $Ca_v1.3$ channel complexes in inner hair cells and is essential for normal hearing (Fell et al., 2016). The $\alpha_2\delta_3$ subunit (CACNA2D3) co-assembles with high voltage-activated $Ca_v2.1$ channel complexes in spiral ganglion neurons and auditory brainstem nuclei and is essential for normal synaptogenesis and auditory processing (Pirone et al., 2014).

Low voltage-activated, T-type Ca_v3 channels also have been identified in the inner ear. $Ca_v3.1$ channels were found in outer hair cells (Inagaki et al., 2008), in ribosome-rich cells of endolymphatic sac epithelia (Cottrell et al., 2018), and in other sensory and non-sensory epithelial cells of the mouse inner ear (Nie et al., 2008). $Ca_v3.2$ appears to be the most highly expressed T-type channel in the cochlea and auditory brainstem and was suggested to play a role in age-related and noise-induced hearing loss (Lundt et al., 2019). The presence

of voltage-activated calcium channels in cells of the inner ear suggests that CACHD1 may be expressed in these cells and complex with and modulate the activity of these channels.

Here, we describe our discovery and analysis of mice with a naturally occurring, recessive *Cachd1* missense mutation (*Cachd1*^{tow}) that, when homozygous, causes inner ear dysfunction. For comparisons, we also analyzed mice homozygous for a targeted CRISPR/Cas9-generated *Cachd1* knockout mutation (*Cachd1*$^{-/-}$) and found that they exhibit the same vestibular-related behaviors and hearing impairment as *Cachd1*$^{tow/tow}$ mice. We show that the hearing impairment of *Cachd1* mutant mice is associated with increased endolymph volume and calcium concentrations and with decreased endocochlear potentials. We also show that the vestibular dysfunction of mutant mice is related to deficiencies of calcium carbonate crystals (otoconia) in the saccule and utricle. These findings support CACHD1 as an $\alpha_2\delta$-like auxiliary subunit of voltage-dependent calcium channels in the inner ear, which modulates endolymph calcium concentrations that are vital for normal auditory and vestibular function.

Materials and methods

Mice

Experimental mice were bred and housed in the Research Animal Facility of the Jackson Laboratory in Bar Harbor, Maine. Post-weaning mice were also shipped to Washington University School of Medicine (WUSM) in St. Louis, Missouri, for additional analyses. All procedures involving the use of experimental mice were approved by the Institutional Animal Care and Use Committees at JAX and WUSM. All methods used in the study were performed in accordance with the guidelines and regulations of the U.S. National Institutes of Health (NIH) Office of Laboratory Animal Welfare (OLAW) and the Public Health Service (PHS) Policy on the Humane Care and Use of Laboratory Animals.

The *Cachd1*^{tow} mutation arose spontaneously in the B6(Cg)-*Bmp5*$^{se-4J}$/J strain (Stock #1496) at JAX. The *Bmp5*$^{se-4J}$ mutation was subsequently removed from the colony, and the *Cachd1*^{tow} mutation is now maintained in a strain designated B6(Cg)-*Cachd1*^{tow}/GRSRKjn, available as JAX Stock # 9689. The strain containing the CRISPR/Cas9-derived *Cachd1* knockout mutation that was developed and analyzed in this study is designated C57BL/6J-*Cachd1*^{em1Kjn}/Kjn, available as JAX Stock # 31290.

Genetic mapping and whole exome sequencing to identify the Cachd1^{tow} mutation

To map the *tow* mutation genetically, individual DNA samples from linkage cross mice were typed for multiple MIT microsatellite markers located throughout the mouse genome. Previously described PCR methods (Johnson et al., 2012) were used to geno-type the chromosomal markers, which were then analyzed for co-segregation with the mutant phenotype (circling behavior). PCR primer pairs designed to amplify specific markers were purchased from Integrated DNA Technologies (Coralville, IA, USA).

Whole-exome sequencing was used to identify the *tow* mutation in the *Cachd1* gene, with focus on the genetically determined candidate gene region. DNA purification, library construction, deep sequencing, and data quality control were performed by the Jackson

Laboratory's Next Generation Sequencing service, and data analysis and annotation were performed by the Computational Sciences-Biostatistics service. Purified genomic DNA from *tow/tow* mice was used to create a library for whole-exome sequence capture. Exon sequences from this library were compared with those of the C57BL/6J reference sequence.

CRISPR/Cas9 generation of the Cachd1^{em1Kjn} mutation

Mice with targeted CRISPR/Cas9 generated deletions of the *Cachd1* gene (strain C57BL/6J-*Cachd1*^{em1Kjn} /Kjn) were produced by the Jackson Laboratory's Genetic Engineering Technologies Service. Two single guide RNAs flanking the targeted region in exon 1 of *Cachd1* were used to generate deletions by non-homologous end joining, and mice with a 98 bp DNA deletion, which also includes a 1 bp insertion (Fig. 2 D), were selected for strain development. Putative founder mice showing deletions of appropriate size and location were crossed to wild-type C57BL/6J mice to produce N1 generation mice. After final characterization of the transmitted alleles in N1 mice, selected individuals were intercrossed to establish a homozygous line with the desired deletion.

Genotyping of the Cachd1^{tow} and Cachd1^{em1Kjn} mutations

Genotypes for the *Cachd1*^{tow} mutation were determined by DNA sequence analysis of PCR products (Fig. 2C). The following PCR primers were used to amplify the exon 23 region of *Cachd1* containing the *tow* mutation: 5′ -CTCCCCACTTGACAAGGAAA-3′ (forward) and 5′-CGCACAGTAGGATTTGTCCA-3′ (reverse), expected to produce a product size of 221 bp. The expected PCR product size was confirmed on a 3.5% agarose gel, and PCR products were purified with the QIAquick PCR Purification Kit (Qiagen Inc., Valencia, CA). The same primers used for PCR amplification were used to sequence the purified PCR products on an Applied Biosystems 3700 DNA Sequencer with an optimized Big Dye Terminator Cycle Sequencing method.

Genotypes for the *Cachd1*^{em1Kjn} mutation were determined from the differently sized PCR products of wild-type and mutant alleles (Fig. 2D). The following PCR primers were used to amplify the exon 1 region of the *Cachd1* gene containing the *em1Kjn* mutation: 5′GCGCCCCCTAAGTTTTCCAG-3′ (forward) and 5′-AAGAGGGGGAAAGTGGGTGC-3′ (reverse). The wild-type allele is expected to produce a product size of 576 bp and the mutant allele a product size of 478 bp, a size difference that is easily resolvable on a 3% agarose gel.

Inner ear whole mount preparations

Newborn (P1) mice were decapitated and half-heads were fixed in Bodian's fixative after the brain was removed. Heads were fixed overnight and then dehydrated with 75% ethanol (2 × 2 hours), 95% ethanol (2 × 2 hours), and 100% ethanol (2 × 2 hours). Heads were then rinsed once with methyl salicylate and cleared overnight by placing specimens in methyl salicylate. To observe otoconia, the cleared inner ears were sub-illuminated and photographed using a Leica dissecting microscope.

Inner ears from three-month-old mice (P87) were dissected and flushed with neutral-buffered formalin (NBF) through a hole made at the cochlear apex. Inner ears were then

immersed in NBF, dehydrated in ethanol, and cleared in methyl salicylate overnight. The preserved whole-mount preparations were examined for abnormalities under a dissecting microscope. To highlight the otolith organs, the cleared inner ears were visualized using polarized light because of its sensitivity to the refractive properties of otoconia.

Inner ear paint-fills

Paint-fills of inner ears were performed using previously described procedures (Kiernan, 2006; Tian et al., 2017). E15.5 mouse embryos were decapitated and the heads bisected and fixed overnight in Bodian's fixative. P0 mice were decapitated and half-heads were fixed in Bodian's fixative after the brain was removed. The heads were then dehydrated in 75% ethanol (2 × 2 hours), 95% ethanol (2 × 2 hours), and 100% ethanol (2 × 2 hours) and cleared overnight in methyl salicylate. Several microliters of 1% Wite-Out correction fluid in methyl salicylate were injected into the middle turn of the cochlea using a Hamilton syringe, with a pulled glass capillary needle broken to a tip diameter of 20–40 μm. For P0 inner ears, a second injection was made in the common cruss. The paint-filled inner ears were then dissected away from the rest of the head.

ABR measures at JAX

At The Jackson Laboratory, ABR thresholds were measured at 8, 16 and 32 kHz in a sound attenuating chamber using the SmartEP auditory evoked potential diagnostic system from Intelligent Hearing Systems (IHS, Miami, FL) as described previously (Zheng et al., 1999). Acoustic stimuli were calibrated into a Bruel and Kjaer 2 cc coupler, Type DB0138, using SmartEP software in conjunction with a Bruel and Kjaer Nexus conditioning amplifier, Type 2690, 1/4 inch calibrated condenser microphone, Type 4136, and microphone preamplifier, Type 2670. Mice were anesthetized with tribromoethanol (0.2 ml of 20 mg/ml stock per 10g body weight, i.p.) and placed on a temperature controlled heating pad to maintain body temperature at 37 °C. Output tubes from high frequency transducers were snugly fit in the ear canals of the mouse. Both ears were tested simultaneously, with the more sensitive ear selected for between-animal comparisons. Three subdermal electrodes, placed at the vertex and behind each ear, were used to record brain stem responses to defined tone-bursts (3 ms duration. 1.5 ms cosine-gated rise/fall time, 19.1/s). Responses were digitized (25 kHz sampling rate, 10 ms analysis window), amplified (200,000x), filtered (100–3000 Hz), and averaged (512 sweeps minimum). Stimulus intensity was initially decreased in 10 dB steps from 90 dB SPL until the response began to disappear and then further lowered in 5 dB steps; ABR threshold was defined as the lowest intensity at which a response could be reliably obtained in 3–5 threshold-crossings. With our testing system, average ABR thresholds for normal hearing mice are about 40, 20, and 45 dB SPL for 8, 16 and 32 kHz stimuli, respectively. Data from ABR tests at JAX are shown in Figs. 1 and 3.

ABR and distortion product otoacoustic emission (DPOAE) measures at WUSM

At Washington University School of Medicine, ABR recordings were obtained from the left ear of 25 *Cachd1* homozygous mutants, 7 heterozygotes and 13 wild-type mice, roughly evenly split by sex. Recordings were carried out in a foam-lined single-walled soundproof room (IAC). Animals were anesthetized (80 mg/kg ketamine, 15 mg/kg xylazine, IP) and positioned dorsal-side-up in a custom head holder. Core temperature was maintained at 37.5

± 1.0 °C using a DC electric heating pad in conjunction with a rectal probe (FHC). Platinum needle electrodes (Grass) were inserted subcutaneously just behind the left ear (active), at the vertex (reference), and in the back (ground). Electrodes were connected to a Grass P55 differential am plifier (300–3,000 Hz, x100), then to a custom amplifier providing another 1,000X gain, then digitized at 30 kHz and visualized using Tucker Davis Technologies (TDT) System 2 hardware and software. Sine wave stimuli having 0.5 ms $\cos^2$ rise/fall times and 5.0 ms total duration were generated and calibrated using TDT System2 hardware and software. Stimuli were presented free-field using TDT ES-1 speakers placed 7.0 cm from the left pinna and calibrated offline using an ACO Pacific 7016 ¼ inch microphone placed where the external auditory meatus would normally be. During ABR tests, tone burst stimuli at each frequency and level were presented up to 1,000 times at 20/sec. The minimum sound pressure level (SPL) required for visual detection of ABR Wave I was determined at 5, 10, 20, 28.3, 40 and 56.6 kHz using a 5 dB minimum step size. Thresholds were confirmed by two threshold-crossings at each test frequency. Data from ABR tests at WUSM are shown in Fig. 8A.

DPOAEs (2f1-f2) were measured from the left ears in sessions separate from ABR recording. 12 *Cachd1* mutant, 7 Het, and 7 WT mice roughly evenly split by sex were prepared as for ABR measures. ‘DP-grams’ were obtained by presenting two tones (f1 and f2, where f1 = f2/1.2) at fixed level differences (L1 and L2, where L2 = L1–10 dB) for f2 ranging 5–40 kHz, and L1 and L2 set at 75 and 65 dB SPL, respectively. Stimuli were presented using TDT EC1 speakers configured in a closed acoustic system along with a Knowles probe microphone to record speaker and cochlear output. Primary and DPOAE levels were recorded using EMAV software in conjunction with TDT and custom hardware.

Endocochlear potential (EP) and endolymph Ca^{2+} measures at WUSM

To record the EP, animals were anesthetized with 60 mg/kg sodium pentobarbital and positioned ventral-side-up. A hole was made in the left cochlear capsule directly over scala media of the lower basal turn, using a fine drill. Glass capillary pipettes (40–80 MΩ) filled with 0.15 M KCl were mounted on a hydraulic microdrive (Frederick Haer) and advanced until a stable positive potential was observed that did not change with increased electrode depth. The signal from the recording electrode was led to an AM Systems Model 1600 intracellular amplifier. EP measures were obtained from 15 *Cachd1* mutant, 7 Het and 6 WT mice in groups roughly evenly split by sex.

Endolymphatic Ca^{2+} levels were measured in series of experiments separate from those used for EP measures (above). 10 *Cachd1* mutant and 5 WT mice were prepared as for EP recording using the left cochlea. Double-barreled pipettes beveled at the tip were fashioned with one barrel containing 0.15 M KCl for EP measuring, and the other containing 500 mM KCl in the barrel and WPI IE200 Ca^{2+} exchange solution in the tip. Pipettes were inserted into the cochlea manually until a stable EP was observed. The electrochemical potential between the Ca^{2+} electrode and electrical ground was calibrated against a series of Ca^{2+} standards, both prior to use and immediately after each recording. Using custom hardware and software, both the EP and Ca^{2+} potential were logged every 10 seconds for a minimum

of 10 measures, which were averaged. Ca^{2+} levels for each animal were determined by comparing cochlear readings with standard curves.

Tissue processing and imaging for histopathology at WUSM

After ABR and EP recordings, animals were overdosed and perfused transcardially with cold 2.0% paraformaldehyde/2.0% glutaraldehyde in 0.1 M phosphate buffer (pH 7.4). Each cochlea was rapidly isolated, immersed in the same fixative, and the stapes was immediately removed. After decalcification in sodium EDTA for 72 hours, cochleae were post-fixed in buffered 1% osmium tetroxide, dehydrated in an ascending acetone series, and embedded in Epon. Cochleae were serial sectioned parallel to the modiolus at 4.0 μm, then stained with toluidine blue for bright field viewing using a Nikon Optiphot light microscope and Nikon NIS Elements software. All auditory and vestibular epithelia were examined qualitatively in left inner ears from 3 *Cachd1* mutant and 3 WT mice. Given the wide range of severity of phenotypes observed in the mutant mice, those selected for examination were among those showing no ABR response at any frequency.

RNA in situ hybridization

Freshly dissected inner ears were fixed in 10% neutral buffered formalin (NBF) for 24 hours at room temperature. After two washes with 1xPBS (pH = 7.4), the samples were dehydrated in a series of ethanol solutions of increasing concentrations (70–100%), cleared by xylene immersion, and embedded in paraffin. 5 μm sections were cut using a microtome (Leica).

In situ hybridizations were performed using the RNAscope Assay (Wang et al., 2012). The *Cachd1* probe was designed by Advanced Cell Diagnostics (ACDBio, USA) and consisted of a cocktail of short 20 bp oligonucleotides spanning the 1419–2346 bp target region of the mouse *Cachd1* mRNA sequence (NM_198037.1). Hybridizations of the *Cachd1* probe and positive and negative control probes were performed with reagents and procedures described in the ACDBio User Manual for the RNAscope 2.5 HD Detection Kit (BROWN) using a Leica BOND autostainer.

Experimental design and statistical analysis

Numbers, sexes, and ages of mice are given for each analysis. All measurements (ABR, DPOAE, EP, Ca^{2+} concentration) were conducted in a blinded and randomized manner. All statistical analyses were run using SigmaPlot. Analyses of group differences consisted of 2-way ANOVAs with Holm-Sidak posthoc multiple comparisons or (for two-sample comparisons) Student's t-test or Mann-Whitney rank sum test. Error bars around means (standard deviations or standard errors) are specified in the figure legends for each graph. For Pearson's correlations, statistical significance of correlation coefficients (r) was determined by comparison with the critical values in a Pearson's correlation table for a given α significance level and number of paired-measures.

Results

Mutant tow/tow mice exhibit vestibular and auditory dysfunction

The average ABR thresholds of 5–12 week old mice that exhibited vestibular deficits (n = 27) were 40–50 dB above those of age-matched mice with normal motor behavior (n = 14) (Fig. 1A). These mean differences were significant by 2-way ANOVA (df = 1, F = 191.672, $p < 0.001$), with no interactions by test frequency. ABR thresholds of all mice with vestibular deficits were elevated but highly variable, with 16 kHz threshold elevations ranging from 20–80 dB above control values (Fig. 1B). A few individuals with normal behavior exhibited elevated ABR thresholds, suggesting that the abnormal vestibular-related behaviors may not be fully penetrant in *tow/tow* mutant mice.

Genetic mapping of the tow mutation and candidate gene analysis

We used a linkage backcross to map the *tow* mutation. Female CAST/Ei-+/+ mice were mated with B6(Cg)-*tow/tow* male mice to produce +/*tow* F1 hybrids, which were then backcrossed to *tow/tow* mutant mice. This backcross was designated (CAST x B6-*tow)* x B6-*tow*. ABR thresholds were measured for the first 120 N2 backcross progeny produced from this cross (Fig. 1C). 16 kHz thresholds that were above 30 dB SPL were considered elevated compared with normal values obtained from age-matched B6 mice. By this criterion, 21 of 28 N2 backcross mice with vestibular-related behavioral abnormalities (75%), and 3 of 92 mice with normal behavior (3%), exhibited elevated ABR thresholds. These results indicate that neither abnormal behavior nor elevated ABR thresholds are fully penetrant phenotypes of *tow/tow* backcross mice. ABR analysis of additional backcross mice with normal behavior was discontinued because most (> 95%) of these mice exhibit normal ABR thresholds (Fig. 1C) and therefore cannot be used to identify *tow/tow* genotypes. A total of 111 backcross mice with abnormal behaviors characteristic of vestibular dysfunction were produced for linkage analysis. The presumed *tow/tow* genotypes of these mice were analyzed for associations with the genotypes of strain-specific polymorphic SNP markers distributed throughout the genome. By haplotype segregation analysis, the *tow* mutation was mapped to a 10 Mb region of Chr 4, between SNP markers rs6197377 (96.7 Mb position, GRCm38) and rs6310620 (106.7 Mb position).

The 10 Mb candidate region of Chr 4 contains about 45 named protein-coding genes. We selected *Bsnd* (106.5 Mb) as a possible candidate gene for the *tow* mutation because the human ortholog, *BSND*, underlies Bartter syndrome with sensorineural deafness (OMIM #602522), and disruption of *Bsnd* in mice causes profound congenital hearing loss (Rickheit et al., 2008). We screened *Bsnd* for mutations by complete genomic DNA sequence analysis of its four exons; however, no sequence differences were found between *tow/tow* mutant and +/+ control mice.

Identification and characterization of the tow mutation in the Cachd1 gene

None of the other genes within the genetically determined candidate region for the *tow* mutation had known attributes that appeared related to the *tow/tow* phenotype, so we used the whole exome sequencing approach in an attempt to identify the underlying mutation. High throughput exome sequencing analysis comparing DNA from *tow/tow* and +/+ mice

identified 164 sequence differences in exons located in the 96.7–106.7 Mb candidate region of Chr 4, but 123 of these were non-causative inbred strain differences (previously identified SNPs or indels). Of the remaining 41 sequence differences, only one, located within the poorly characterized cache domain containing 1 gene (*Cachd1*; Fig. 2A,B) was predicted to have a negative functional consequence. This detrimental mutation is a single nucleotide base change from G to A in exon 23 of *Cachd1* (Fig. 2 C). The mutation (c.3158 G > A) changes a highly conserved codon for cysteine (TGC) to that of tyrosine (TAA) at amino acid position 1053 of the protein (p.C1053Y). The PolyPhen-2 program (Adzhubei et al., 2013) predicts that the equivalent missense mutation in the human protein is very likely damaging with the maximum score of 1.000. Additional *tow/tow* (n = 6) and non-mutant control mice (n = 4) from the colony were genotyped for the *Cachd1* mutation by DNA sequencing of PCR products, and in all cases genotypes and phenotypes agreed, further confirming the causative nature of the mutation.

Generation of a targeted Cachd1 knockout allele and phenotypic comparisons with Cachd1$^{tow/tow}$ mice

We used CRISPR/Cas9 gene editing to generate a knockout (KO) allele of *Cachd1* and selected a mutant line with a 98 bp out-of-frame deletion in exon 1 to serve as the founder line for the mutation, designated *Cachd1*^{em1Kjn} (Fig. 2D). The phenotype of the homozygous *Cachd1*^{em1Kjn} KO mouse (hereafter referred to as *Cachd1*$^{-/-}$) appears the same as that of the *Cachd1*$^{tow/tow}$ mouse, verifying that *tow* is indeed an allelic mutation of the *Cachd1* gene. DNA typing methods (Fig. 2 C,D) allowed us to assign unambiguous *Cachd1* genotypes to mice without reference to their phenotypes.

Cachd1$^{tow/tow}$ and *Cachd1*$^{-/-}$ mutant mice showed similar hearing thresholds. Mean ABR thresholds of the 72 *Cachd1*$^{tow/tow}$ mutants and 82 *Cachd1*$^{-/-}$ mutants examined were very similar and did not differ statistically (Fig. 3A). The hearing loss of *Cachd1*$^{tow/tow}$ and *Cachd1*$^{-/-}$ mutant mice is highly variable and does not progress from 1–6 months of age (Fig. 3B). When *Cachd1*$^{tow/tow}$ and *Cachd1*$^{-/-}$ mutant mice were further classified by circling phenotype (Fig. 3C), circlers were found to have significantly higher ABR thresholds than non-circlers by 2-way ANOVA ($df = 2$, $F = 140.536$, $p < 0.001$) with no interactions by test frequency. Although subtle balance deficits may have gone unnoticed in some of the mutants, we observed that about 45% of *Cachd1*$^{tow/tow}$ (32/72; Fig. 3D) and *Cachd1*$^{-/-}$ (37/82; Fig. 3E) mice exhibited overt circling and head tilting behaviors.

No sex differences were apparent in the ABR thresholds of mutant mice by 2-way ANOVA at any frequency (data not shown). Mean ABR thresholds for the total 88 female and 66 male *Cachd1*$^{tow/tow}$ and *Cachd1*$^{-/-}$ mutant mice were 65.1 for females and 61.7 for males at 8 kHz, 46.9 for females and 45.8 for males at 16 kHz, and 67.0 for females and 64.8 for males at 32 kHz.

Morphological analyses of inner ears from Cachd1 mutant mice

We further examined *Cachd1* mutant mice for inner ear pathologies that may account for their characteristic vestibular dysfunction (circling and head tilting behavior, reported failure to swim) and hearing impairment. Microscopic examinations of cleared, whole mount

preparations of inner ears from newborn *Cachd1*$^{-/-}$ and 3-month-old *Cachd1*$^{tow/tow}$ mutant mice revealed variable deficiencies of otoconia in the saccule and utricle (Fig. 4), which could account, at least in part, for the abnormal balance behaviors observed in many of these mutant mice.

To compare inner ear morphologies in more detail, we examined paint-filled membranous labyrinths of inner ears from E15.5 embryos (1 wild type, 3 heterozygotes, and 7 homozygous mutants) and P0 newborn mice (1 wild type, 2 heterozygotes, and 4 homozygous mutants), with examples shown in Fig. 5. When compared with inner ears of control mice (Fig. 5 A,B,E), the inner ears of *Cachd1*$^{-/-}$ mutant mice showed variable degrees of dilation of the membranous labyrinth, from extensive (Fig. 5D,H) and intermediate (Fig. 5C,G) levels of expansion to normal appearing (Fig. 5F). The endolymphatic duct, utricle, saccule, and cochlear duct all appeared enlarged in inner ears of E15.5 mutant mice (Fig. 5C,D), although this did not appear to apply to the endolymphatic sac. The endolymphatic sac did not always fill with paint in inner ears of P0 mice but when it could be observed in mutant mice it did not appear swollen (Fig. 5G).

Inner ear histopathology

Cross-sections of plastic-embedded cochleae showed differences in the arrangement of cochlear fluid spaces in *Cachd1* mutant and WT mice. These differences prominently included lateral expansion of fluid spaces (transverse to the modiolus), basal displacement of the organ of Corti, and reduction in size of scala tympani in the mutants (Fig. 6A,B). Scala media appeared expanded, as indicated by displacement of Reissners membrane toward scala vestibuli. Most noteworthy was the partial or complete absence of the boney interscalar septum between the lower cochlear basal and apical turn (compare arrows in Fig. 6A,B). In the mutant animals examined, the organ of Corti of the basal turn was highly atrophic (Compare region marked by arrow in Fig. 6C,E). Outer hair cells appeared almost entirely absent in the basal turn, but some were seen in the apical turn. Inner hair cells appeared somewhat preserved in the mutants, particularly in the apical turn, as were most afferent neurons. The tectorial membrane varied in appearance in the mutants from near-normal to displaced or completely absent. In the example shown (Fig. 6E), the tectorial membrane appears displaced and encased in connective tissue. The spiral ligament appeared attenuated in the mutants throughout the cochlea (Compare Fig. 6D,F), particularly in the basal turn. The structure of stria vascularis appeared largely preserved in the mutants, although differences in strial volume by genotype could not be ruled out.

Comparison of the vestibular organs by genotype (Fig. 7) indicated little hair cell or neural loss in the *Cachd1* mutants. All mutant cristae appeared similar to those of WTs, including the presence of dark cells (Fig. 7A,C). The status of the cupulae could not be determined due to typical fixation artifacts in this structure. The appearance of the macular epithelia was likewise similar between genotypes with respect to hair cells. However, among the six otolith organs (maculae) examined in three mutant mice, only a single saccule contained any otoconia at all, in this case a single large and misshapen profile (Fig. 7D). Based on appearance, it is possible that *Cachd1* mutant cristae would function normally if K^+ levels are normal, since the endolymphatic potential is normally low in the vestibular organs. The

maculae, however, are likely un-responsive due to the lack of normal otoconia, despite little apparent hair cell loss.

The histological analyses of inner ears from *Cachd1* mutant mice described above focused on those that had the greatest hearing loss. In general, however, the severity of inner ear pathology was quite variable among *Cachd1* mutant mice (Extended Data Fig. 6–1), consistent with the variability seen among hearing thresholds and vestibular motor behaviors.

Additional measures of cochlear function in Cachd1$^{-/-}$ knockout mice

ABR, DPOAE, and EP measures were obtained at WUSM on *Cachd1*$^{-/-}$ and control mice sent from JAX. ABR thresholds for 25 mutant and 20 control (heterozygote and wild-type) mice (Fig. 8A) showed an overall significant effect of genotype ($df = 2$, $F = 123.135$, $p < 0.001$), whereby heterozygote and wild-type mice differed significantly from *Cachd1*$^{-/-}$ mice at all test frequencies, but from each other only at 40 kHz ($t = 2.389$, $p = 0.018$). ABR threshold averages in mutant mice were about 50 dB higher than those of control mice at 5–28.3 kHz. Thresholds were more mixed for 40 and 56.6 kHz test stimuli, likely because the *Cdh23* variant of the B6 background strain confers a highly variable, accelerated, hearing loss at higher frequencies.

DPOAE data (Fig. 8B) showed a significant effect of genotype ($df = 2$, $F = 43.039$, $p < 0.001$) by 2-way ANOVA (limited to ABR test frequencies), with interactions by f2 frequency. Overall, *Cachd1*$^{-/-}$ mice showed significantly smaller responses than heterozygotes or wild-type mice ($t = 6.481$, 8.560, respectively, $p < 0.001$). Heterozygotes and wild-type mice differed significantly at f2 = 10 kHz ($t = 2.06$, $p = 0.042$), likely reflecting the typical scatter of DPOAE measures in even young B6 mice.

EP values in individual *Cachd1* mutant mice varied widely (4–107 mV), with 10 out of 16 showing values below the typical normal range for B6 (Fig. 8C). In contrast, EP measurements of heterozygous and wild-type mice were consistently high (94–111 mV). Median EPs of non-mutant (103.0 mV) and mutant (46.0 mV) mice were significantly different ($t = 275.000$, $p < 0.001$, Mann-Whitney rank sum test).

ABR thresholds and EPs in mutant mice and were negatively correlated (Fig. 8D), with 16 paired measures giving a Pearson correlation coefficient (r) of −0.885 and a coefficient of determination (R^2) of 0.783 for the correlation of EP with ABR thresholds at 20 kHz. The negative correlation was significant at a two-tail significance level of $p = 0.001$. DPOAEs for f2 = 20 kHz and ABR thresholds at 20 kHz were also negatively correlated (not shown), with 12 paired measures giving a correlation coefficient of −0.628, which is significant at a two-tail significance level of $p = 0.05$. There was no significant correlation between DPOAEs (for f2 = 20 kHz) and EP measures, although only 8 paired-measures were tested.

Elevated Ca^{2+} concentrations in cochlear endolymph of Cachd1$^{-/-}$ knockout mice

The recent identification of CACHD1 as an auxiliary subunit that modulates the activity of voltage-gated calcium channels (Cottrell et al., 2018; Dahimene et al., 2018; Stephens and Cottrell, 2019) prompted us to examine endolymph Ca^{2+} concentrations in additional

Cachd1$^{-/-}$ mutant mice and *Cachd1*$^{+/+}$ control mice sent from JAX to WUSM for testing (Fig. 9). In the mouse, endolymphatic ion concentrations reach mature levels during the first postnatal week.

Cochlear endolymph Ca^{2+} concentrations (Fig. 9A) varied widely among mutant mice. The mean value for mutant mice (179.4 μM) was significantly greater than for wild-type mice (56.3 μM), with a two-tail Student's t-test probability of 0.013 (t = −2.882, df = 12.715). EPs were measured at the same time in the same mice to test for associations with the endolymph Ca^{2+} measures (Fig. 9B). The EP mean for mutant mice (78.8 mV) was significantly lower than for control mice (102.1 mV), with a two-tail Student's t-test probability of 0.024 (df = 12.584, t = 2.561). EP measures and Ca^{2+} concentrations were significantly negatively correlated (Fig. 9C), with a Pearson correlation coefficient (r) of −0.60 and a coefficient of determination (R^2) of 0.36. The correlation coefficient obtained from 15 paired-measures was statistically significant at a two-tail significance level of 0.02.

Expression of Cachd1 in the inner ear

We used mRNA *in situ* hybridization to examine *Cachd1* expression in B6 wild-type mice. *Cachd1* expression was weak in cochleae of 1-month-old mice (Fig. 10A) and could be positively identified only in a few cells at higher magnification (Extended Data Fig. 10–1). *Cachd1* expression, however, was readily apparent in the cochlear ducts of E14.5 (Fig. 10B) and E16.5 (Fig. 10C,D) embryos, especially in the thickened epithelium along the floor of the cochlear duct in E14.5 embryos (Fig. 1B). We were unable to obtain identifiable sections through the vestibular regions of the embryonic inner ear for *in situ* hybridization analysis.

Discussion

CACHD1 recently was shown to be an alpha2 delta ($\alpha_2\delta_1$)-like ancillary subunit that modulates Ca_v3 T-type channels (Cottrell et al., 2018) and that can compete with $\alpha_2\delta_1$ subunits to increase $Ca_v2.2$ channel currents (Dahimene et al., 2018). These studies also demonstrated that CACHD1 facilitates the cell surface localization and activity of these voltage-gated calcium channels in the central nervous system and in neuronal cell cultures. Here, we show that CACHD1 also functions in the inner ear and that mice with mutations of *Cachd1* are hearing impaired and have balance defects. Voltage-gated Ca^{2+} channels have been found in other regions of the inner ear in addition to inner hair cell synapses, including marginal cells of the stria vascularis (Inui et al., 2007; Mori et al., 2009), which have been postulated to play a role in regulating the EP (Mori et al., 2009), and in vestibular dark cells (Imon et al., 1997; Mori et al., 1998). Less polarized secretory epithelial cells may be more likely to have low-voltage activated calcium channels like T-type Ca_v3 channels, which are proposed to complex with CACHD1 (Cottrell et al., 2018), in contrast to the high-voltage activated L-type Ca_v1 channels of highly polarized hair cells (Nakaya et al., 2007).

The inner ear dysfunctions of mutant mice are associated with increased ABR thresholds, endolymph Ca^{2+} concentrations, and endolymph volume, with decreases in EP and DPOAE responses, and with deficiencies of otoconia in the utricle and saccule. All of these associations potentially can be attributed to a calcium dysregulation in the inner ear. The decreased DPOAEs of *Cachd1* mutant mice (Fig. 8B) indicate that the amplification function

of outer hair cells is diminished by CACHD1 deficiency. The ~50 dB elevations in ABR thresholds of *Cachd1* mutant mice (Figs. 1A, 3, 8A) are consistent with the 40–60 dB decrease in cochlear sensitivity caused by the loss of OHC motility in prestin-deficient mutant mice (Liberman et al., 2002). The loss of OHC function could therefore explain most of the ABR threshold increases seen in *Cachd1* mutant mice and explain the strong negative correlation of DPOAE and ABR thresholds. Reduced OHC function may be a consequence of decreased EP (Fig. 8C), which would diminish the intensity of hair cell responses to auditory stimuli and explain the negative correlation of ABR thresholds with EP (Fig. 8D).

The membranous labyrinths of *Cachd1*$^{-/-}$ mutant embryos exhibited variable degrees of dilation, from extensive to normal appearing (Fig. 5), and cross sections of cochleae from adult mice did not all show an expanded scala media (Fig. 6–1). This variability in endolymph volume is similar to, and may be related to, the variability seen in ABR thresholds, DPOAE measurements, EP recordings, and endolymph calcium concentrations of these mice (Figs. 8, 9). High calcium concentrations in endolymph have been associated with endolymphatic hydrops (Meyer zum Gottesberge and Ninoyu, 1987; Meyer zum Gottesberge, 1988; Salt et al., 1989; Salt and DeMott, 1994; Salt and Plontke, 2010). Increased Ca^{2+}-ATPase activity in the cochlear lateral wall following induction of hydrops also suggests a relationship of disturbed calcium homeostasis with inner ear hydrops (Hsu et al., 2001). We observed a similar association of Ca^{2+} and endolymph volume in *Cachd1* mutant mice. An increase in endolymph Ca^{2+} concentration in adult cochleae (Fig. 8) is associated with expansion of the scala media in adult mice (Fig. 6 and Fig. 6–1) and dilation of the membranous labyrinth in embryonic inner ears (Fig. 5).

Recently, the low-voltage gated T-type calcium channel $Ca_v3.2$ and the epithelial sodium channel ENaC were shown to have overlapping expression patterns and to functionally interact, suggesting that they may reciprocally regulate each other's trafficking and channel activities (Garcia-Caballero et al., 2019). $Ca_v3.2$ is the most highly expressed T-type channel in the cochlea (Lundt et al., 2019). Because Na^+ transport is one of the most important driving forces in fluid transport, ENaC is thought to play an important role in regulating endolymph volume in the inner ear (Kim et al., 2014). The role of CACHD1 as an auxiliary subunit that regulates T-type calcium channels (Cottrell et al., 2018) suggests that it may have an indirect effect on ENaC activity and inner ear fluid dynamics, which may relate to the excess endolymph volume we observed in *Cachd1* mutant mice.

Curiously, the endolymphatic sac of *Cachd1*$^{-/-}$ mutant inner ears at E15.5 and P0 is not enlarged (Fig. 5), in contrast to the greatly swollen endolymphatic sac of mice with mutations of other genes that cause dilations of the membranous labyrinth, including *Atp6v1b1*$^{vtx/vtx}$ (Tian et al., 2017), *Atp6v0a4*$^{-/-}$ (Lorente-Canovas et al., 2012), *Foxi1*$^{-/-}$ (Hulander et al., 2003), and *Slc26a4*$^{-/-}$ (Everett et al., 2001) mutant mice, where the increase in endolymph volume is caused by the failure of epithelial cells of the endolymphatic sac to remove excess fluid. The non-expanded size of the endolymphatic sac in inner ears of *Cachd1*$^{-/-}$ mice suggests that the increased volume of endolymph in these mice may be the result of an increase in endolymph fluid production from epithelial cells lining the lumen rather than by a decrease in fluid resorption at the endolymphatic sac. Fluid secretion in the embryonic inner ear is poorly understood because mechanisms of ion

transport and fluid composition that have been established in adults were finalized during the first postnatal week and cannot be extrapolated to embryos (Kim and Wangemann, 2010). *Cachd1* expression in mice appears to be stronger in the cochlear ducts of E14.5 and E16.5 embryos than in adults (Fig. 10). This temporal pattern of expression suggests that CACHD1 plays a more important role in the establishment of the ionic composition of inner ear fluids in embryos rather than in their maintenance in adults.

Otoconia are bio-crystals of calcium carbonate that add mass to the membrane overlying the sensory maculae of the utricle and saccule of the inner ear. They couple mechanical forces to hair cell transduction to sense linear acceleration and gravity, essential for maintaining balance. The otoconial deficiencies of *Cachd1* mutant mice are similar to those observed in mice lacking otopetrin 1 (OTOP1), which was shown to regulate cellular calcium in vestibular supporting cells (Kim et al., 2010) and in mice lacking the AT-Pase plasma membrane Ca^{2+} pump 2 (ATP2B2), which also is involved in inner ear calcium regulation (Kozel et al., 1998). Extracellular bio-mineralization of otoconia requires establishing the correct concentrations of calcium, carbonate, and hydrogen ions localized above the utricular and saccular maculae (Hughes et al., 2006; Lundberg et al., 2006; Lundberg et al., 2015). CACHD1 may modulate voltage-gated calcium channels that contribute to the establishment of proper calcium concentrations in regions of otoconia formation.

This is the first report of a *Cachd1* mutant phenotype and the first evidence for the involvement of CACHD1 in inner ear function. We show that endolymph Ca^{2+} concentrations are correlated with EPs (Fig. 9), EPs and DPOAEs are correlated with ABR thresholds (Fig. 8), and ABR thresholds are correlated with vestibular dysfunction (Fig. 3) in *Cachd1* mutant mice. Our results are consistent with CACHD1 functioning as an auxiliary subunit of voltage dependent calcium channels in the inner ear that help to maintain calcium homeostasis, which is critical for normal auditory and vestibular function. Balance behaviors, ABR thresholds, endolymph volume increases, DPOAEs, EPs, and endolymph Ca^{2+} concentrations all exhibited a high degree of variability in *Cachd1* mutant mice. This variability may be related to CACHD1's role as an $\alpha_2\delta$–like subunit that modulates rather than controls voltage-gated calcium channel function. Endolymphatic hydrops, observed in the *Cachd1* mutant mice, is frequently associated with Menière's disease, an inner ear condition characterized by spontaneous episodes of vertigo, fluctuating sensorineural hearing loss, aural fullness, and tinnitus (Gürkov et al., 2016). Increased $[Ca^{2+}]$ in the endolymph is a shared pathology among Menière's disease, experimental endolymphatic hydrops, and space motion sickness (Meyer zum Gottesberge and Ninoyu, 1987). The variable degree of hearing loss and vestibular phenotype in *Cachd1* mutant mice bears similarity to the symptoms seen in Menière's patients. Enlarged vestibular aqueduct syndrome (EVAS) is another common inner ear condition associated with an enlarged endolymphatic duct, also causing hearing loss and balance symptoms (Smith et al., 1998). Given that *Cachd1* mutant mice recapitulate symptoms seen in Menière's and EVAS, for which the etiology is largely unknown, these mice may usefully model such conditions.

Supplementary Material

Refer to Web version on PubMed Central for supplementary material.

Acknowledgements

This work was supported by the National Institutes of Health (NIH) grants R01-DC004301 (to K.R.J) and P30-CA034196 (Jackson Laboratory shared services). We thank Chantal Longo-Guess for ABR tests of linkage cross mice, Sandra Gray for mouse husbandry, and the shared services of The Jackson Laboratory for whole exome sequencing, generation of mice with CRISPR-Cas9 mutations, and strain cryopreservation.

References

Adzhubei I, Jordan DM, Sunyaev SR, 2013. Predicting functional effect of human missense mutations using PolyPhen-2. Curr. Protoc. Hum. Genet Chap. 7 Unit7 20.

Anantharaman V, Aravind L, 2000. Cache - a signaling domain common to animal Ca(2+)-channel subunits and a class of prokaryotic chemotaxis receptors. Trends Biochem. Sci. 25, 535–537. [PubMed: 11084361]

Brandt A, Striessnig J, Moser T, 2003. $Ca_V1.3$ channels are essential for development and presynaptic activity of cochlear inner hair cells. J. Neurosci. 23, 10832–10840. [PubMed: 14645476]

Cottrell GS, Soubrane CH, Hounshell JA, Lin H, Owenson V, Rigby M, Cox PJ, Barker BS, Ottolini M, Ince S, Bauer CC, Perez-Reyes E, Patel MK, Stevens EB, Stephens GJ, 2018. CACHD1 is an alpha2delta-like protein that modulates Ca_V3 voltage-gated calcium channel activity. J. Neurosci. 38, 9186–9201. [PubMed: 30181139]

Dahimene S, Page KM, Kadurin I, Ferron L, Ho DY, Powell GT, Pratt WS, Wilson SW, Dolphin AC, 2018. The alpha2delta-like protein Cachd1 Increases N-type calcium currents and cell surface expression and competes with alpha2delta-1. Cell Rep. 25, 1610–1621 e1615. [PubMed: 30404013]

Davies A, Hendrich J, Van Minh AT, Wratten J, Douglas L, Dolphin AC, 2007. Functional biology of the alpha(2)delta subunits of voltage-gated calcium channels. Trends Pharmacol. Sci. 28, 220–228. [PubMed: 17403543]

Dolphin AC, 2016. Voltage-gated calcium channels and their auxiliary sub-units: physiology and pathophysiology and pharmacology. J. Physiol. 594, 5369–5390. [PubMed: 27273705]

Everett LA, Belyantseva IA, Noben-Trauth K, Cantos R, Chen A, Thakkar SI, Hoogstraten-Miller SL, Kachar B, Wu DK, Green ED, 2001. Targeted disruption of mouse Pds provides insight about the inner-ear defects encountered in Pendred syndrome. Hum. Mol. Genet. 10, 153–161. [PubMed: 11152663]

Fell B, Eckrich S, Blum K, Eckrich T, Hecker D, Obermair GJ, Munkner S, Flockerzi V, Schick B, Engel J, 2016. alpha2delta2 controls the function and trans-synaptic coupling of $Ca_V1.3$ channels in mouse inner hair cells and is essential for normal hearing. J. Neurosci. 36, 11024–11036. [PubMed: 27798183]

Garcia-Caballero A, Gandini MA, Huang S, Chen L, Souza IA, Dang YL, Stutts MJ, Zamponi GW, 2019. $Ca_V3.2$ calcium channel interactions with the epithelial sodium channel ENaC. Mol. Brain 12, 12. [PubMed: 30736831]

Gürkov R, Pyykö I, Zou J, Kentala E, 2016. What is Meniere's disease? A contemporary re-evaluation of endolymphatic hydrops. J. Neurol. 263, 71–81.

Hsu CJ, Tan CT, Shau WY, Chen YS, Yeh TH, SY Lin-Shiau, 2001. Na+,K+-ATPase and Ca^{2+} -ATPase activities in the cochlear lateral wall following surgical induction of hydrops. Hear. Res. 156, 95–103. [PubMed: 11377885]

Hughes I, Thalmann I, Thalmann R, Ornitz DM, 2006. Mixing model systems: using zebrafish and mouse inner ear mutants and other organ systems to unravel the mystery of otoconial development. Brain Res. 1091, 58–74. [PubMed: 16529728]

Hulander M, Kiernan AE, Blomqvist SR, Carlsson P, Samuelsson EJ, Johansson BR, Steel KP, Enerback S, 2003. Lack of pendrin expression leads to deafness and expansion of the endolymphatic compartment in inner ears of Foxi1 null mutant mice. Development 130, 2013–2025. [PubMed: 12642503]

Imon K, Amano T, Ishihara K, Sasa M, Yajin K, 1997. Existence of voltage-dependent Ca^{2+} channels in vestibular dark cells: cytochemical and whole-cell patch–clamp studies. Eur. Arch. oto-rhino-Laryngol. 254, 287–291.

Inagaki A, Ugawa S, Yamamura H, Murakami S, Shimada S, 2008. The $Ca_V3.1$ T-type Ca^{2+} channel contributes to voltage-dependent calcium currents in rat outer hair cells. Brain Res. 1201, 68–77. [PubMed: 18294617]

Inui T, Mori Y, Watanabe M, Takamaki A, Yamaji J, Sohma Y, Yoshida R, Takenaka H, Kubota T, 2007. Physiological role of L-type Ca^{2+} channels in marginal cells in the stria vascularis of guinea pigs. J. Physiol. Sci. 57, 287–298. [PubMed: 17963592]

Johnson KR, Longo-Guess CM, Gagnon LH, 2012. Mutations of the mouse ELMO domain containing 1 gene (Elmod1) link small GTPase signaling to actin cytoskeleton dynamics in hair cell stereocilia. PLoS One 7, e36074.

Kiernan AE, 2006. The paintfill method as a tool for analyzing the three-dimensional structure of the inner ear. Brain Res. 1091, 270–276. [PubMed: 16600188]

Kim BG, Kim JY, Kim HN, Bok J, Namkung W, Choi JY, Kim SH, 2014. Developmental changes of ENaC expression and function in the inner ear of pendrin knock-out mice as a perspective on the development of endolymphatic hydrops. PLoS One 9, e95730.

Kim E, Hyrc KL, Speck J, Lundberg YW, Salles FT, Kachar B, Goldberg MP, Warchol ME, Ornitz DM, 2010. Regulation of cellular calcium in vestibular supporting cells by otopetrin 1. J. Neurophysiol. 104, 3439–3450. [PubMed: 20554841]

Kim HM, Wangemann P, 2010. Failure of fluid absorption in the endolymphatic sac initiates cochlear enlargement that leads to deafness in mice lacking pendrin expression. PLoS One 5, e14041.

Kozel PJ, Friedman RA, Erway LC, Yamoah EN, Liu LH, Riddle T, Duffy JJ, Doetschman T, Miller ML, Cardell EL, Shull GE, 1998. Balance and hearing deficits in mice with a null mutation in the gene encoding plasma membrane Ca^{2+}-ATPase isoform 2. J. Biol. Chem. 273, 18693–18696. [PubMed: 9668038]

Liberman MC, Gao J, He DZ, Wu X, Jia S, Zuo J, 2002. Prestin is required for electromotility of the outer hair cell and for the cochlear amplifier. Nature 419, 300–304. [PubMed: 12239568]

Lorente-Canovas B, Ingham N, Norgett EE, Golder ZJ, Karet Frankl FE, Steel KP, 2012. Mice deficient in the H+-ATPase a4 subunit have severe hearing impairment associated with enlarged endolymphatic compartments within the inner ear. Dis. Model. Mech..

Lundberg YW, Zhao X, Yamoah EN, 2006. Assembly of the otoconia complex to the macular sensory epithelium of the vestibule. Brain Res. 1091, 47–57. [PubMed: 16600187]

Lundberg YW, Xu Y, Thiessen KD, Kramer KL, 2015. Mechanisms of otoconia and otolith development. Developmental dynamics: an official publication of the. Am. Associat. Anatomist. 244, 239–253.

Lundt A, Seidel R, Soos J, Henseler C, Muller R, Bakki M, Arshaad MI, Ehninger D, Hescheler J, Sachinidis A, Broich K, Wormuth C, Papazoglou A, Weiergraber M, 2019. $Ca_V3.2$ T-Type Calcium Channels are Physiologically Mandatory for the Auditory System. Neuroscience.

Lv P, Kim HJ, Lee JH, Sihn CR, Fathabad Gharaie S, Mousavi-Nik A, Wang W, Wang HG, Gratton MA, Doyle KJ, Zhang XD, Chiamvimonvat N, Yamoah EN, 2014. Genetic, cellular, and functional evidence for Ca 2 + inflow through $Ca_V1.2$ and $Ca_V1.3$ channels in murine spiral ganglion neurons. J. Neurosci. 34, 7383–7393. [PubMed: 24849370]

Meyer zum Gottesberge AM, 1988. Imbalanced calcium homeostasis and endolymphatic hydrops. Acta Otolaryngol. Suppl. 460, 18–27. [PubMed: 3074617]

Meyer zum Gottesberge AM, Ninoyu O, 1987. A new aspect in pathogenesis of experimental hydrops: role of calcium. Aviat. Space Environ. Med. 58, A240–A246. [PubMed: 3675500]

Mori Y, Amano T, Sasa M, Yajin K, 1998. Cytochemical and patch-clamp studies of calcium influx through voltage-dependent Ca^{2+} channels in vestibular supporting cells of guinea pigs. Eur. Arch. oto-rhino-Laryngol. 255, 235–239.

Mori Y, Watanabe M, Inui T, Nimura Y, Araki M, Miyamoto M, Takenaka H, Kubota T, 2009. Ca(2+) regulation of endocochlear potential in marginal cells. J Physiol Sci 59, 355–365. [PubMed: 19504169]

Nakaya K, Harbidge DG, Wangemann P, Schultz BD, Green ED, Wall SM, Marcus DC, 2007. Lack of pendrin HCO3-transport elevates vestibular endolymphatic [Ca^{2+}] by inhibition of acid-sensitive TRPV5 and TRPV6 channels. Am. J. Physiol. Ren. Physiol. 292, F1314–F1321.

Nie L, Zhu J, Gratton MA, Liao A, Mu KJ, Nonner W, Richardson GP, Yamoah EN, 2008. Molecular identity and functional properties of a novel T-type Ca^{2+} channel cloned from the sensory epithelia of the mouse inner ear. J. Neurophysiol. 100, 2287–2299. [PubMed: 18753322]

Pirone A, Kurt S, Zuccotti A, Ruttiger L, Pilz P, Brown DH, Franz C, Schweizer M, Rust MB, Rubsamen R, Friauf E, Knipper M, Engel J, 2014. alpha2delta3 is essential for normal structure and function of auditory nerve synapses and is a novel candidate for auditory processing disorders. J. Neurosci. 34, 434–445. [PubMed: 24403143]

Platzer J, Engel J, Schrott-Fischer A, Stephan K, Bova S, Chen H, Zheng H, Striessnig J, 2000. Congenital deafness and sinoatrial node dysfunction in mice lacking class D L-type Ca^{2+} channels. Cell 102, 89–97. [PubMed: 10929716]

Rickheit G, Maier H, Strenzke N, Andreescu CE, De Zeeuw CI, Muenscher A, Zdebik AA, Jentsch TJ, 2008. Endocochlear potential depends on Cl-channels: mechanism underlying deafness in Bartter syndrome IV. Embo. J. 27, 2907–2917. [PubMed: 18833191]

Salt AN, DeMott J, 1994. Endolymph calcium increases with time after surgical induction of hydrops in guinea-pigs. Hear. Res. 74, 115–121. [PubMed: 8040082]

Salt AN, Plontke SK, 2010. Endolymphatic hydrops: pathophysiology and experimental models. Otolaryngol. Clin. North Am. 43, 971–983. [PubMed: 20713237]

Salt AN, Inamura N, Thalmann R, Vora A, 1989. Calcium gradients in inner ear endolymph. Am. J. Otolaryngol. 10, 371–375. [PubMed: 2596623]

Smith RJH, Iwasa Y, Schaefer AM, 1998. Pendred syndrome/nonsyndromic enlarged vestibular aqueduct. In: Adam MP, Ardinger HH, Pagon RA, Wallace SE, Bean LJH, Stephens K, Amemiya A (Eds.), GeneReviews. University of Washington Press, Seattle, pp. 1993–2020.

Stephens GJ, Cottrell GS, 2019. CACHD1: a new activity-modifying protein for voltage-gated calcium channels. Channels 13, 120–123. [PubMed: 30983497]

Tian C, Gagnon LH, Longo-Guess C, Korstanje R, Sheehan SM, Ohlemiller KK, Schrader AD, Lett JM, Johnson KR, 2017. Hearing loss without overt metabolic acidosis in ATP6V1B1 deficient MRL mice, a new genetic model for non-syndromic deafness with enlarged vestibular aqueducts. Hum. Mol. Genet. 26, 3722–3735. [PubMed: 28934385]

Wang F, Flanagan J, Su N, Wang LC, Bui S, Nielson A, Wu X, Vo HT, Ma XJ, Luo Y, 2012. RNAscope: a novel in situ RNA analysis platform for formalin-fixed, paraffin-embedded tissues. J. Mol. Diagn. 14, 22–29. [PubMed: 22166544]

Zheng QY, Johnson KR, Erway LC, 1999. Assessment of hearing in 80 inbred strains of mice by ABR threshold analyses. Hear. Res. 130, 94–107. [PubMed: 10320101]

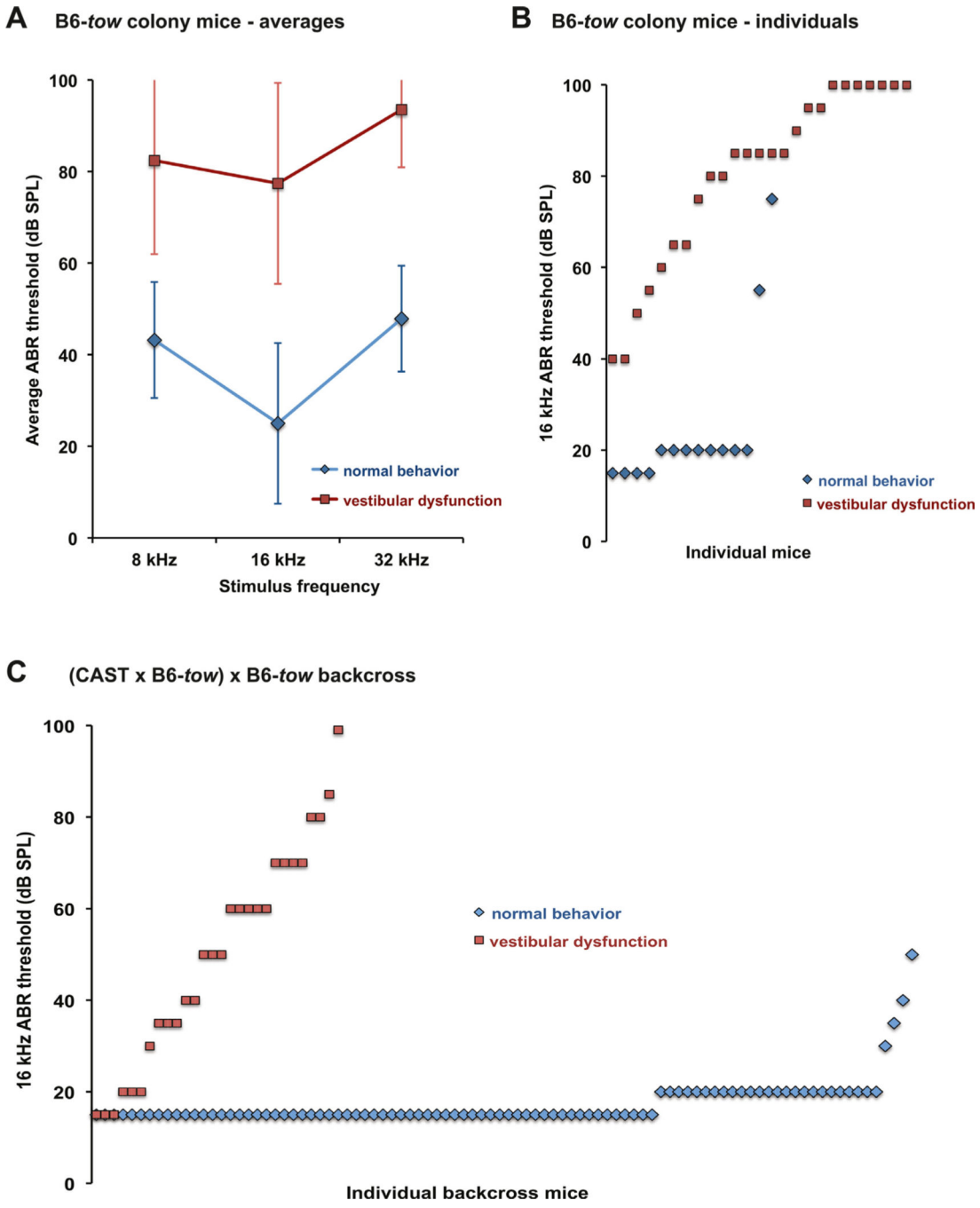

Fig. 1. Mutant *tow/tow* mice exhibit vestibular dysfunction and hearing impairment.

Fourteen mice (8 females, 6 males) with normal behavior and 27 mice (16 females, 11 males) mice with behaviors characteristic of vestibular dysfunction (presumed *tow/tow* genotype) were assessed for hearing by ABR analysis at 5–12 weeks of age. **(A)** ABR threshold averages of B6-*tow* colony mice. Threshold averages of mice with vestibular dysfunction were about 40–50 dB higher than those of mice with normal behavior at all test frequencies. These differences were significant by 2-way ANOVA (df = 1, F = 191.672, $p < 0.001$), with no interactions by frequency. Bars indicate standard deviations. **(B)** 16 kHz

ABR thresholds of individual B6-*tow* colony mice. All mice with vestibular dysfunction exhibited elevated 16 kHz ABR thresholds (> 30 dB SPL) as compared with B6 control mice, but the thresholds were highly variable (ranging from 40–100 dB SPL). Two mice with normal behavior exhibited elevated ABR thresholds. **(C)** 16 kHz ABR thresholds of 120 individual N2 mice from the (B6-*tow* x CAST) x B6-*tow* linkage backcross measured at 4–7 weeks of age. Ninety-two of these mice (45 females, 47 males) had normal behavior, and 28 (12 females, 16 males) showed behaviors characteristic of vestibular dysfunction. The 16 kHz thresholds of the mice with normal behavior varied from 15–50 dB SPL (average value 17), with three of the mice exhibiting elevated thresholds (> 30 dB SPL). Thresholds of the mice with vestibular dysfunction varied from 15–100 dB SPL (average value 50), with seven of the mice exhibiting normal thresholds (< 35 dB SPL).

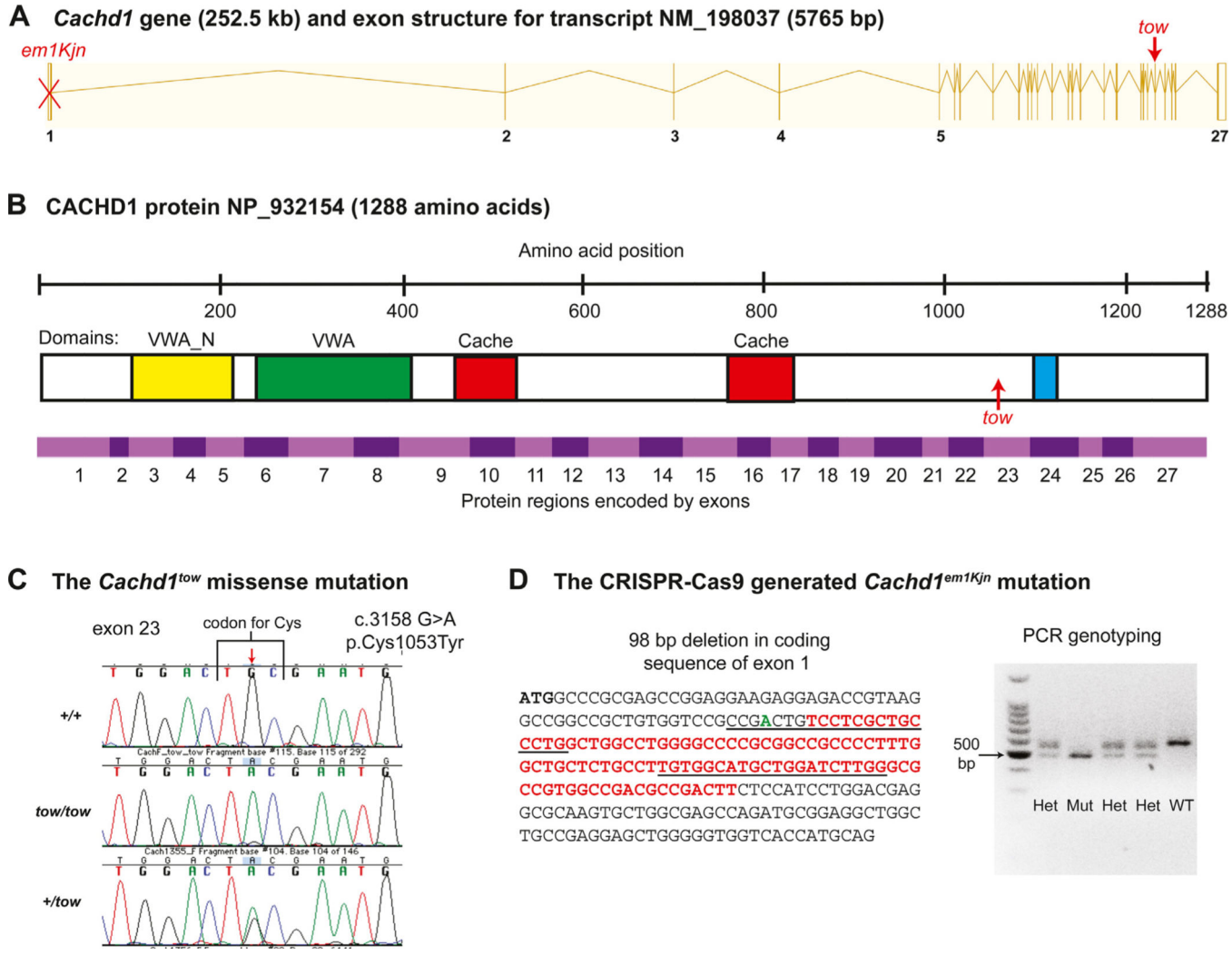

Fig. 2. Structure of the mouse *Cachd1* gene, protein domains, and mutations.

(A) Exon structure of the *Cachd1* gene. The CRISPR/Cas9-generated *em1Kjn* knockout mutation, marked by a red X, is a deletion within exon 1. A red arrow marks the position of the spontaneous *tow* missense mutation in exon 23. **(B)** Domains of the CACHD1 protein. Amino acid positions are shown above the protein diagram. The green rectangle indicates the position of the von Willebrand factor domain (VWA), the yellow rectangle the N-terminal VWA domain (VWA_N), the two red rectangles the cache domains, and the blue rectangle the transmembrane domain (TM). An upward pointing arrow indicates the position of the *tow* missense mutation. Alternating pink and purple bands below the protein diagram indicate the regions of the protein encoded by each of the 27 exons of the *Cachd1* gene. **(C)** The spontaneous $Cachd1^{tow}$ missense mutation. A single base pair substitution at nucleotide position 3158 of the cDNA coding sequence (c.3158 G > A), indicated by the downward pointing red arrow, changes a TGC codon for cysteine to a TAC codon for tyrosine at amino acid position 1053 (p.Cys1053Tyr). Genotyping of mice for the $Cachd1^{tow}$ mutation was performed by DNA sequence analysis of PCR products as shown by the chromatogram. **(D)** The CRISPR-Cas9 generated $Cachd1^{em1Kjn}$ deletion mutation.

The mutation deleted 98 bp (sequence shown in red font) within the protein-coding region of exon 1, and inserted a single bp (shown in green font). Recognition sequences for the two guide RNAs are underlined. Genotyping of mice for the *Cachd1*^{em1Kjn} mutation is easily accomplished by agarose gel electrophoresis to distinguish the sizes of allele-specific PCR products: wild-type (WT) = 576 bp, mutant (Mut) = 478 bp, and heterozygote (Het) = 576 bp, 478 bp. A 100 bp DNA size ladder is shown in the left-most lane.

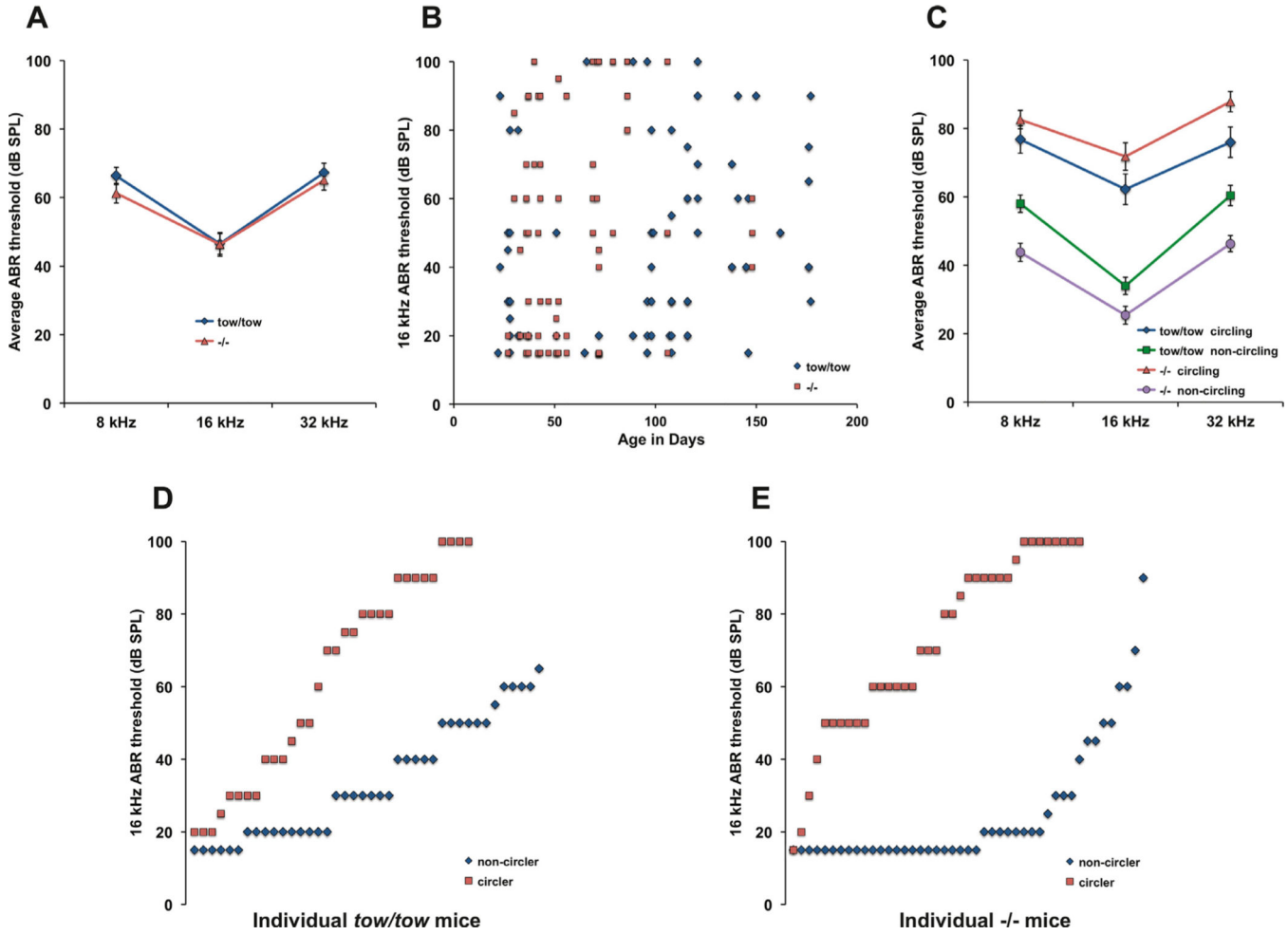

Fig. 3. Hearing thresholds and vestibular-related behavior of *Cachd1*$^{tow/tow}$ and *Cachd1*$^{-/-}$ mice.

A. *Cachd1*$^{tow/tow}$ and *Cachd1*$^{-/-}$ mice exhibit similar degrees of hearing impairment. ABR mean thresholds of 72 *Cachd1*$^{tow/tow}$ and 82 *Cachd1*$^{-/-}$ mice were not significantly different by 2-way ANOVA. **B.** Hearing impairment in *Cachd1*$^{tow/tow}$ and *Cachd1*$^{-/-}$ mice is highly variable and non-progressive. **C.** Average ABR thresholds of mutant mice with circling behavior were significantly higher than those of mutants with normal motor behavior by 2-way ANOVA ($df = 2$, $F = 140.536$, $p < 0.001$) with no interactions by test frequency. **D, E.** 16 kHz ABR thresholds of individual *Cachd1*$^{tow/tow}$ and *Cachd1*$^{-/-}$ mice illustrate the degree of threshold variability and penetrance of circling behavior among mutant mice.

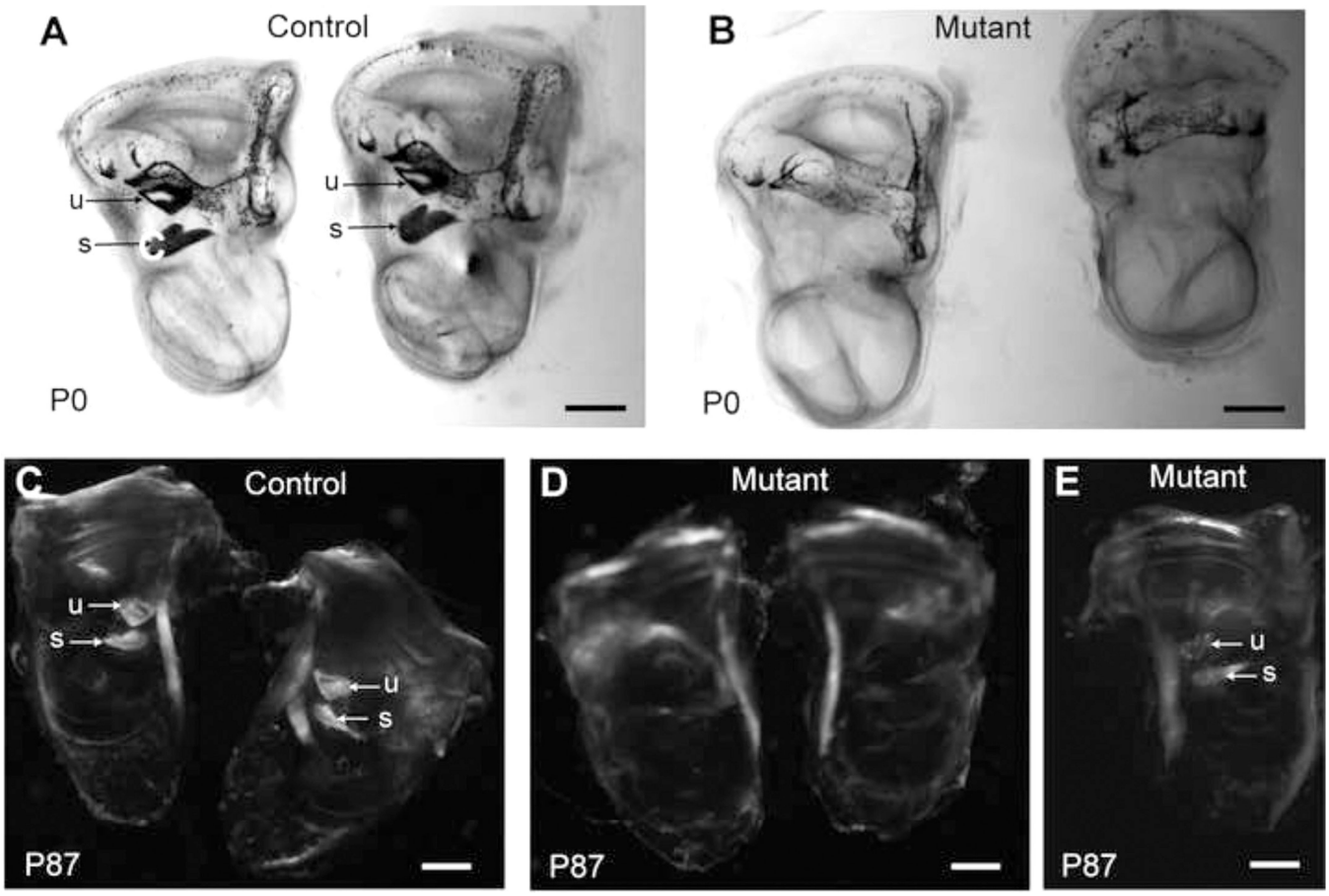

Fig. 4. Otoconia deficiencies in inner ears of *Cachd1* mutant mice.

Cleared, whole mounts of inner ears from B6-+/+ (control) and *Cachd1*$^{-/-}$ knockout (mutant) mice were examined at birth (P0), and inner ears from B6-+/+ (control) and *Cachd1*$^{tow/tow}$ (mutant) mice were examined at 3 months of age (P87). Left and right cleared inner ears of P0 mice **(A, B)** were illuminated from below so that light-blocking calcium carbonate crystals (otoconia) embedded in the membranes overlying the utricule (u) and saccule (s) would appear dark, as seen in controls (arrows in A) but not in mutant mice (B), which appear to lack these crystals. Cleared inner ears of P87 mice **(C, D, E)** were exposed to polarized light to accentuate the calcium carbonate crystals embedded in the otoconial membranes of the utricle (u) and saccule (s), which can clearly be seen in the control ears (arrows, C). Some mutant ears appeared to completely lack otoconia (D) while others showed deficiencies (E).

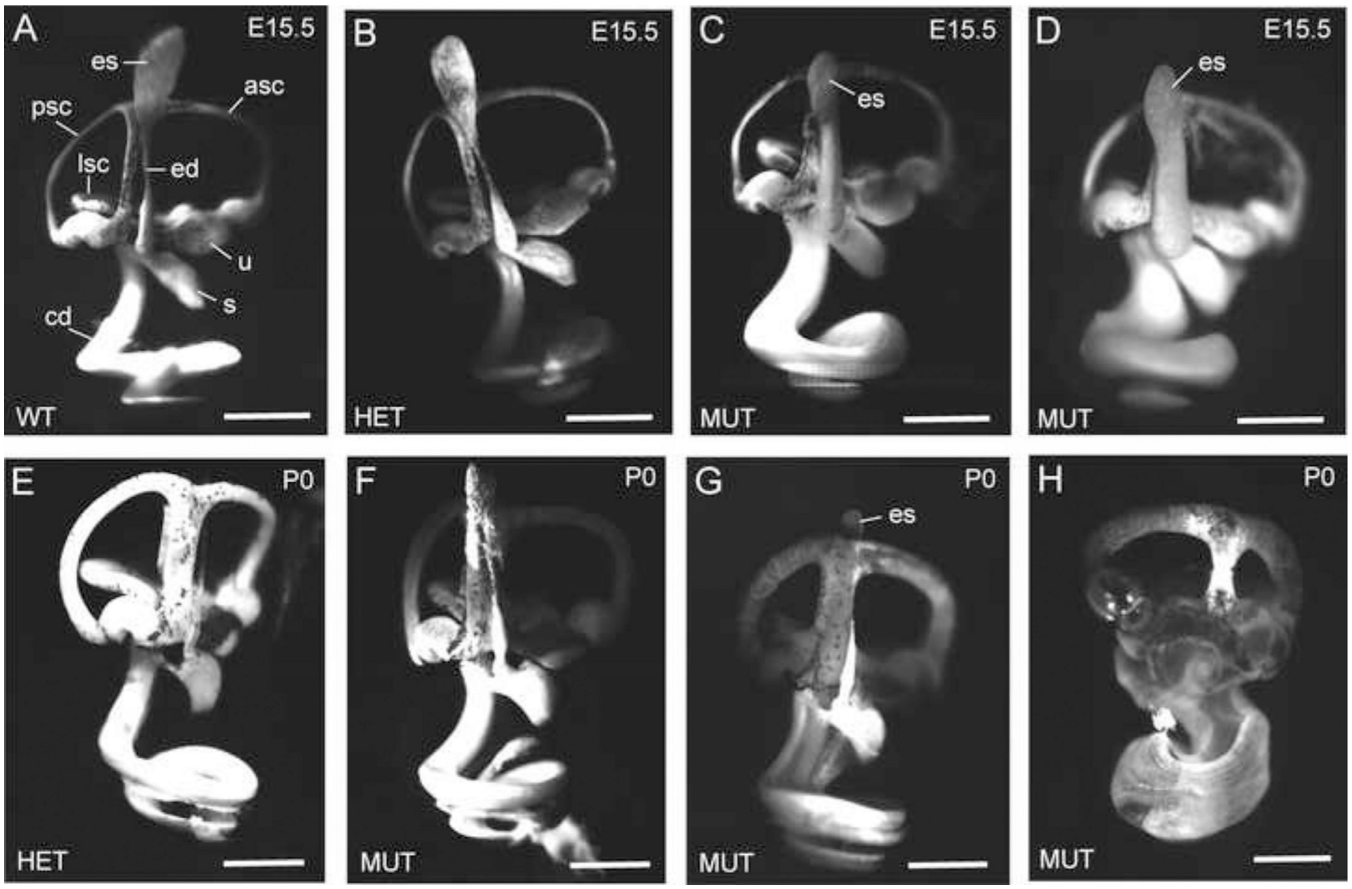

Fig. 5. Paint-fills show dilation of the membranous labyrinth in *Cachd1*$^{-/-}$ E15.5 embryos.

Paint-fills of the membranous labyrinths of inner ears from E15.5-stage embryos (A-D) and P0 newborn mice (E-H) with wild-type (WT, *Cachd1*+/+), heterozygous (HET, *Cachd1*+/−), and homozygous mutant (MUT, *Cachd1*$^{-/-}$) genotypes. For structural reference, the endolymphatic sac (es), endolymphatic duct (ed), utricle (u), saccule (s), cochlear duct (cd), anterior semicircular canal (asc), posterior semicircular canal (psc), and lateral semicircular canal (lsc) are labeled in the wild-type control (A). Inner ears of heterozygous mice (B) appear the same as homozygotes (A), as expected for a recessive trait. At E15.5, the membranous labyrinth of mutant inner ears (C, D) is swollen from an excess of endolymph; however, the endolymphatic sac appears no larger than that of control mice. The degree of labyrinth dilation varied among mutant ears, with some being greatly swollen (D, H), some intermediate (C, G), and some appearing normal (F). Scale bars, 0.5 mm.

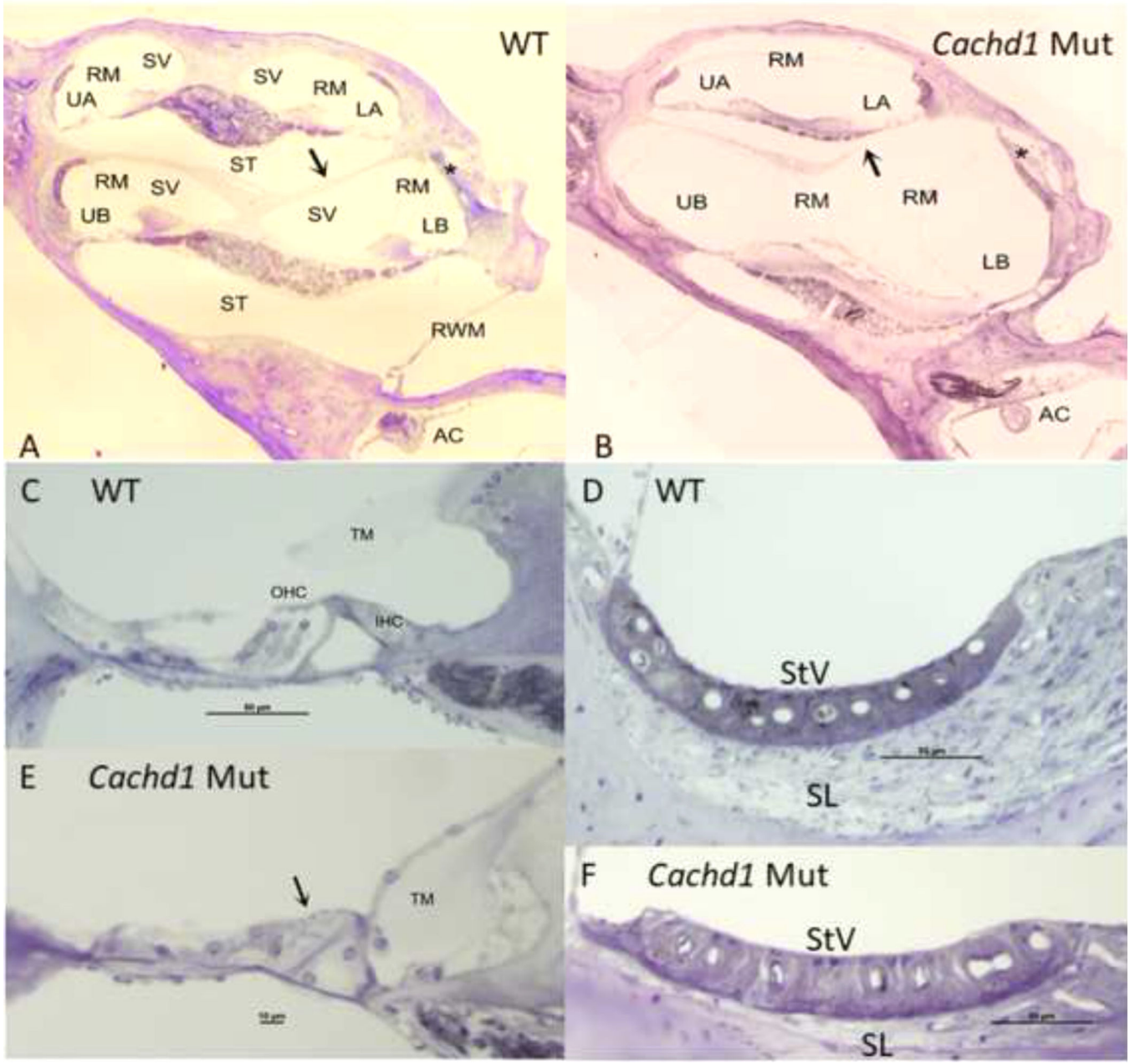

Fig. 6. Whole cochlea comparisons by genotype.

A,B. Cochlear capsule is similarly shaped in *CachD1* mutants and WT mice, but cochlear scala are re-arranged in the mutants, such that scala tympani is reduced in size and scala media is expanded. The boney interscalar septum (arrows in A,B) is partially absent in the mutant shown, and was entirely missing in some animals. Appearance of lower basal turn lateral wall is an artifact related to EP recording (stars in A,B). **C,E.** Normal appearing organ of Corti in WT mouse compared to highly atrophic organ in mutant. Arrow in 4E indicates absence of hair cells in basal turn. Tectorial membrane in mutant is displaced and surrounded by connective tissue. **D,F.** Structure of stria vascularis is similar in mutant and WT, but spiral ligament is much thinner in mutant. AC: Anterior cristae; IHC: Inner hair

cell; LB: Lower base; LA: Lower apex; OHC: Outer hair cells; RM: Reissners membrane; RWM: Round window membrane; ST: Scala tympani; SL: Spiral ligament; StV: Stria vascularis; TM: Tectorial membrane; UA: Upper apex; UB: Upper base.

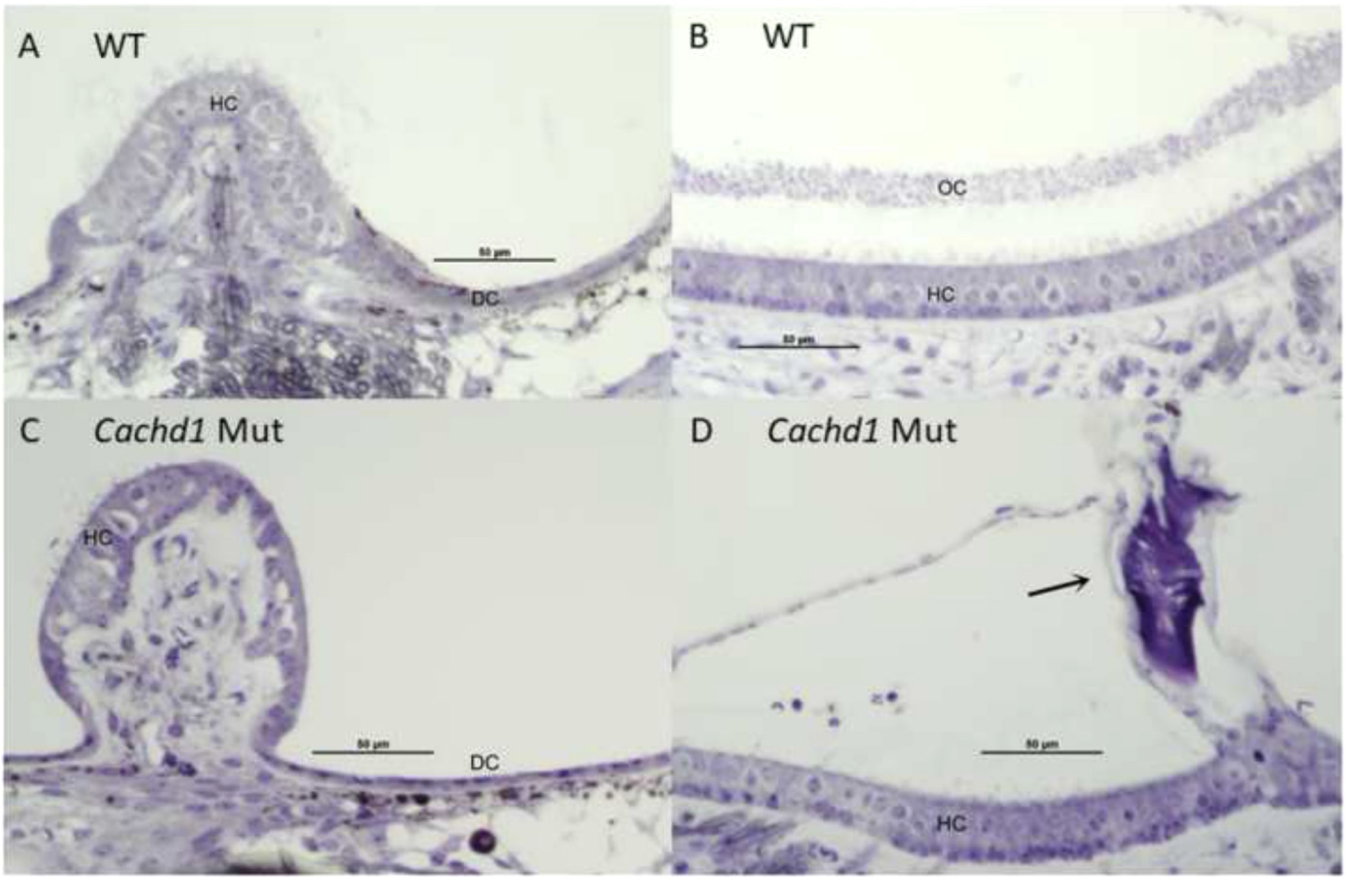

Fig. 7. Maculae and cristae comparisons by genotype.

A,C. No differences were observed among all cristae by genotype, with similar-appearing numbers of hair cells and dark cells. Anterior cristae is shown. **B,D.** Overall structure of all maculae was similar in *Cachd1* mutant and WT mice, with similar appearance of hair cells. However, among six maculae examined in three mutants, only a single, highly abnormal otoconia was found (arrow in D). Saccule is shown. A few artifactual red blood cells appear above the macula in D. DC: Dark cells; HC: Hair cells.

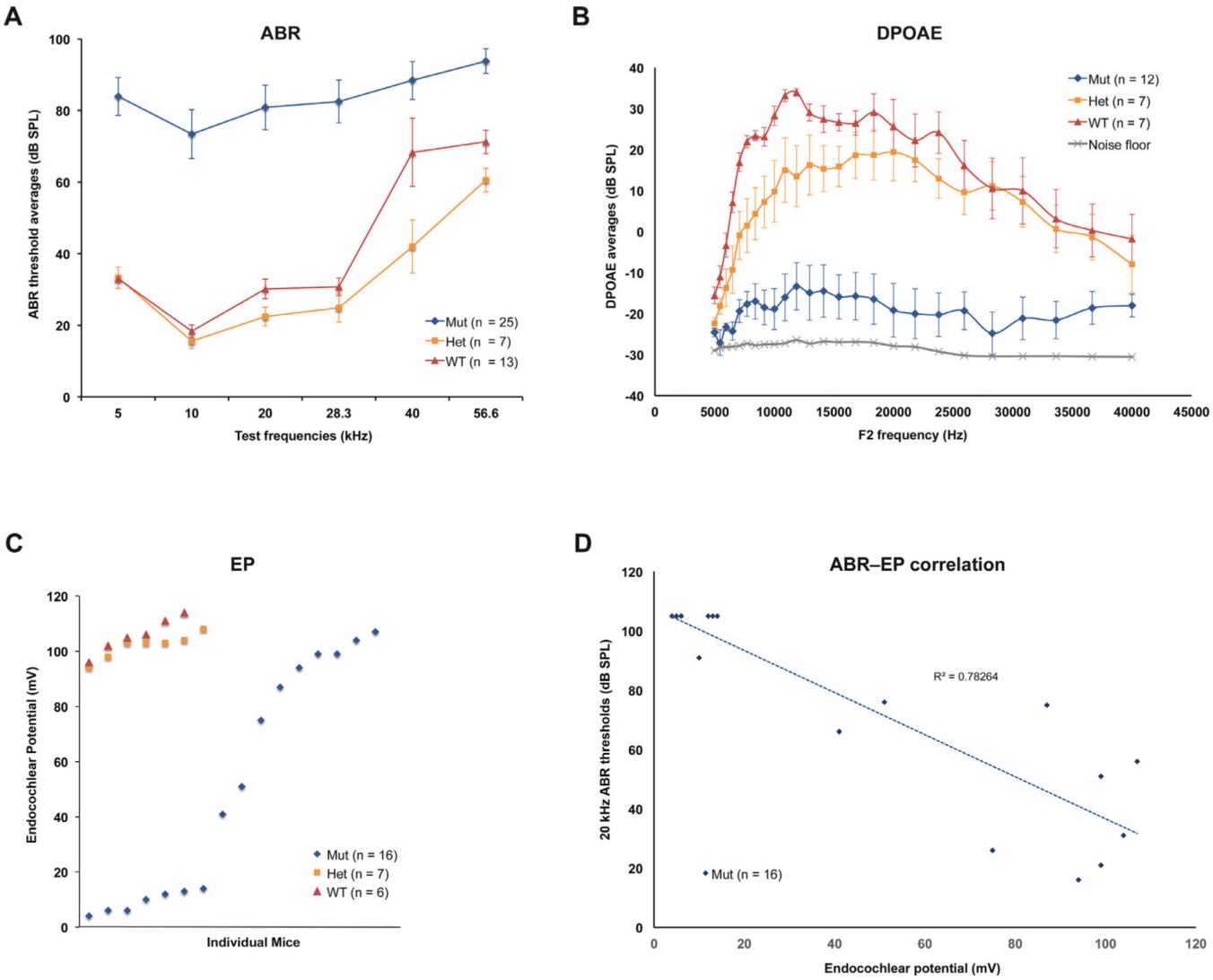

Fig. 8. ABR, DPOAE, and EP measures in *Cachd1*$^{-/-}$ knockout and control mice.

ABR, DPOAE (2f1-f2), and EP measurements at WUSM were made on *Cachd1*$^{-/-}$ mutants (Mut), *Cachd1*$^{+/-}$ heterozygotes (Het), and *Cachd1*$^{+/+}$ wild-type (WT) mice when they were between 2.5 and 4 months of age. **(A)** ABR thresholds for mutant and control (heterozygote and wild-type) mice showed a significant effect of genotype ($df = 2$, $F = 123.135$, $p < 0.001$), whereby heterozygote and wild-type mice differed from *Cachd1*$^{-/-}$ at all test frequencies, but from each other only at 40 kHz ($t = 2.389$, $p = 0.018$). Bars indicate one standard error of the mean. **(B)** DPOAEs showed a significant effect of genotype ($df = 2$, $F = 43.039$, $p < 0.001$) by 2-way ANOVA (limited to ABR test frequencies), with interactions by f2 frequency. Overall, *Cachd1*$^{-/-}$ mice showed smaller responses than heterozygotes or wild-type mice ($t = 6.481$, 8.560, respectively, $p < 0.001$). Heterozygotes and wild-type mice differed significantly at f2 = 10 kHz ($t = 2.06$, $p = 0.042$). Bars indicate one standard error of the mean. **(C)** EP values in *Cachd1* mutant mice varied widely (4–107 mV) while EP measurements of heterozygous and wild-type mice were consistently high (94–111 mV). Median EPs of non-mutant (103.0 mV) and mutant mice (46.0 mV) were significantly

different (t = 275.000, p < 0.0 01, Mann-Whitney rank sum test). **(D)** ABR thresholds and EPs in mutant mice were negatively correlated, with a Pearson correlation coefficient (*r*) of −0.88 for 20 kHz thresholds. The absolute value of *r* (0.88) is higher than the critical *r* value (0.74) for 16 paired measures (df = 14) and a two-tailed significance level of 0.001.

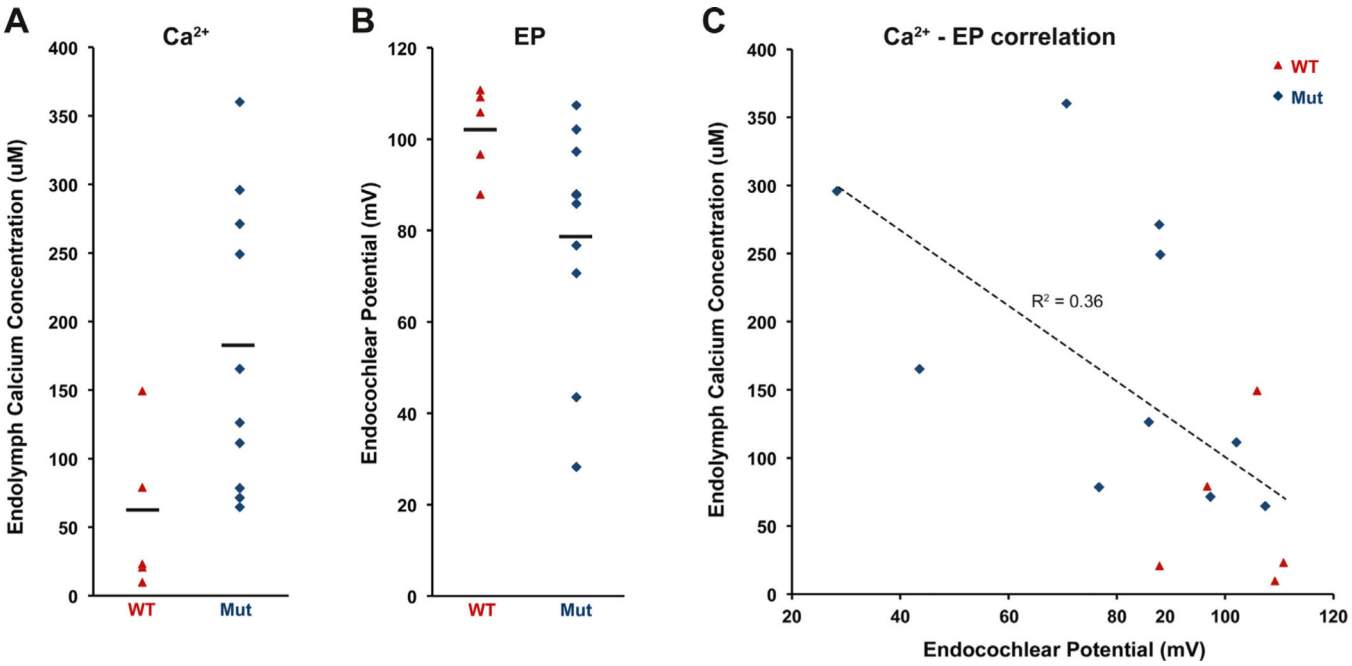

Fig. 9.

Calcium and EP measurements in cochlear endolymph of *Cachd1*$^{-/-}$ mice. Endolymph Ca^{2+} concentrations and EPs were measured in cochleae of 10 *Cachd1*$^{-/-}$ mutants (Mut) and 5 *Cachd1*$^{+/+}$ wild-type (WT) mice at 3–4.5 months of age. **(A)** Cochlear endolymph Ca^{2+} concentrations varied widely among mutant mice. The mean value for mutant mice (179.4 μM) was significantly greater than for wild-type mice (56.3 μM), with a two-tail Student's t-test probability of 0.013 (t = −2.882, df = 12.715). **(B)** EPs measured in the same mice. The EP mean for mutant mice (78.8 mV) was significantly lower than for control mice (102.1 mV), with a two-tail Student's t-test probability of 0.024 (df = 12.584, t = 2.561). **(C)** Ca^{2+} concentrations and EP measurements were negatively correlated, with a Pearson correlation coefficient (r) of −0.60. The absolute value of r (0.60) is higher than the critical r value (0.59) for 15 paired measures (df = 13) and a two-tailed significance level of 0.02.

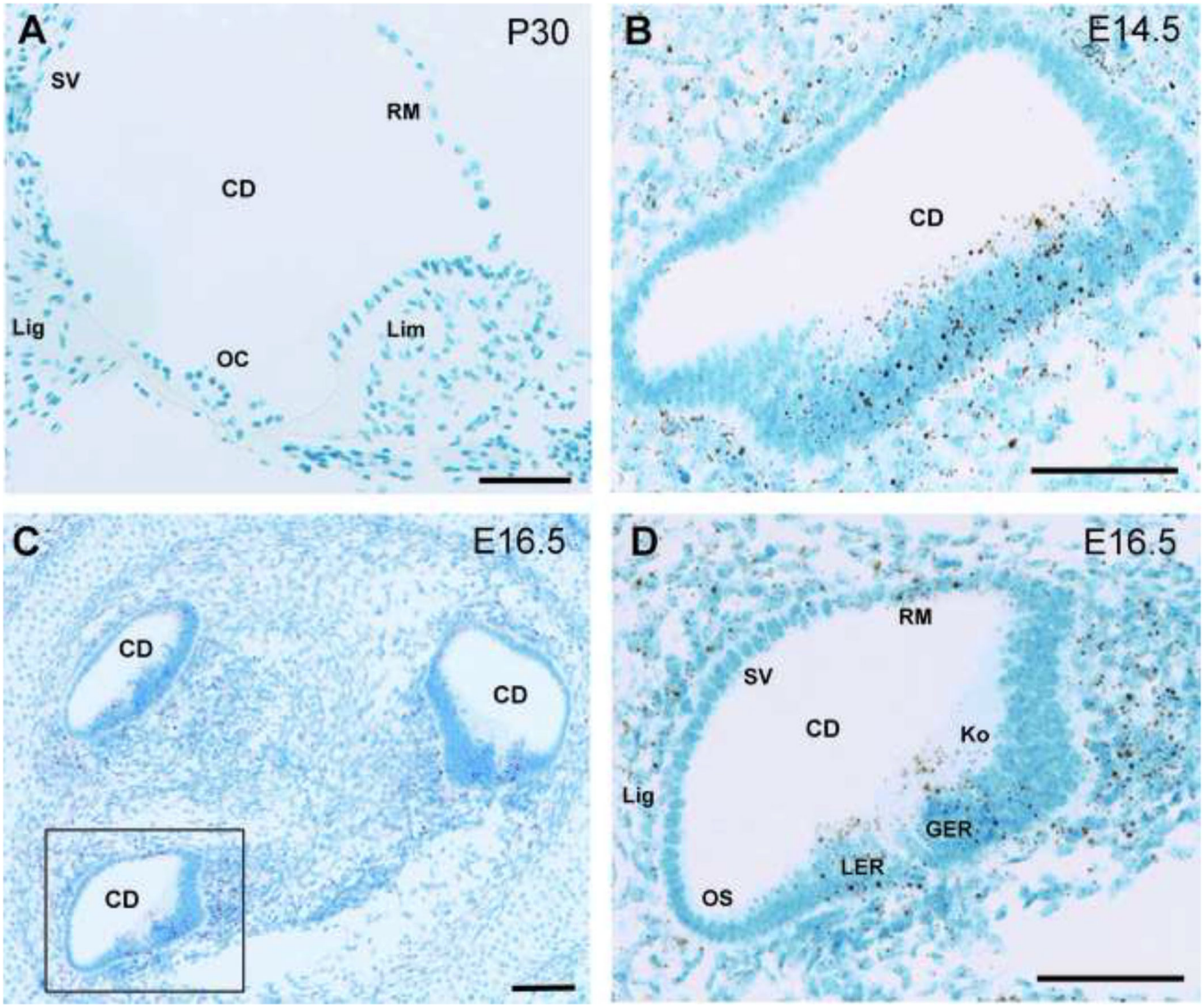

Fig. 10.

Cachd1 expression in the cochleae of embryos and adult mice. *In situ* hybridization results showing *Cachd1* mRNA expression in cross sections through cochlear ducts (CD) of B6 wild-type mice at postnatal day 30 (P30, A) and embryonic days 14.5 (E14.5, B) and 16.5 (E16.5, C and D). Areas of positive *Cachd1* expression are stained brown with a blue counter stain (Hematoxylin). *Cachd1* expression is very weak at P30 (A) and could be positively identified only in a few cells at higher magnification (Extended Data supporting Fig. 1, labeled as Fig. 10–1). Expression is much higher at E14.5 (B), especially in the thickened epithelium along the dorsal side (floor) of the cochlear duct. A section through three turns of the E16.5 cochlea is shown in panel C, with the boxed area shown at higher magnification in panel D. For orientation, regions of the epithelia surrounding the cochlear duct in D are labeled to indicate sites of future cellular structures: stria vascularis (SV), Reissner's membrane (RM), spiral ligament (Lig), and outer sulcus (OS). *Cachd1* expression at E16.5 (D) can be seen in cells of the future Reissner's membrane and in cells comprising

the lesser epithelial ridge (LER) and the greater epithelial ridge (GER), which includes Kolliker's organ (Ko).